Assimilation of future SWOT-based river elevations, surface extent observations and discharge estimations into uncertain global hydrological models

Sly Wongchuig-Correa, Rodrigo Cauduro Dias de Paiva, Sylvain Biancamaria, Walter Collischonn

Assimilation of future SWOT-based river elevations, surface extent observations and discharge estimations into uncertain global hydrological models

Sly Wongchuig-Correa[a,b*], Rodrigo Cauduro Dias de Paiva[a], Sylvain Biancamaria[c], Walter Collischonn[a]

[a] Instituto de Pesquisas Hidráulicas IPH, Universidade Federal do Rio Grande do Sul UFRGS, Brazil

[b] Univ. Grenoble Alpes, IRD, CNRS, Grenoble INP, Institut des Géosciences de l'Environnement (IGE, UMR 5001), 38000, Grenoble, France

[c] CNRS, LEGOS, UMR 5566-CNRS-CNES-IRD-Université Toulouse III, 31057 Toulouse, France

* Author to whom correspondence should be addressed.

Correspondence to: Sly Wongchuig C.

Email: xinox010@gmail.com, +33 (07) 66653687

Published in *Journal of Hydrology* (2020), https://doi.org/10.1016/j.jhydrol.2020.125473

Abstract

Global estimates of river dynamics are needed in order to manage water resources, mainly in developing countries where in-situ observation is limited. Remote sensors such as nadir altimeters can complement ground data. Current altimeters miss however a large number of continental surface water bodies. This issue will be largely resolved by the future Surface Water and Ocean Topography (SWOT) mission, thanks to its wide swath altimeter. SWOT will provide almost globally two-dimensional water elevation maps for rivers over 100 m wide and water bodies over 250 m x 250 m. During this research, we investigated the potential of SWOT to correct hydrological models on a global/continental scale, through data assimilation. For this purpose, an Observing System Simulation Experiment (OSSE), also known as "twin experiment", has been implemented. Model forcings and parameters were perturbed to jointly achieve global hydrological models (GHMs) uncertainties, which is the expected scenario in which the SWOT community will mainly evaluate the future SWOT data. SWOT-like observations of water surface elevation (WSE), flooded water extent (FWE), and/or SWOT derived discharge (Q) were used to correct modelled Q, WSE and FWE from a large-scale hydrological and hydrodynamic model (MGB – portuguese acronym of "Modelo de Grandes Bacias"), using a Ensemble Kalman filter (EnKF). The results indicate that SWOT products could largely improve hydrological simulations on a global and continental scale. SWOT-like discharge can reduce ~40% of model errors in daily discharge. Furthermore, when anomalies of the WSE DA approach were implemented, the error reduction was even greater for all state variables compared to the absolute WSE DA, achieving average error reduction values of about ~30% compared to ~24%. Finally, the simultaneous DA of all the SWOT-like variables together reduces errors from ~14% to ~22% compared to the average of assimilating only one variable.

Keywords: Continental Modeling; Global hydrological model; Data Assimilation; Observing System Simulation Experiment; Surface Water and Ocean Topography.

Published in *Journal of Hydrology* (2020), https://doi.org/10.1016/j.jhydrol.2020.125473

1. Introduction

Continents play a key role in the water cycle yet, due to the vast heterogeneity of continent surface and soil composition, water storage and fluxes are difficult to estimate. Water mass is extremely dependent of soil properties in its different layers, surface topography, vegetation, past runoff which shapes current lakes, river networks and wetlands, human activity (e.g. dams, irrigation, weir), climate zones, and so forth. This complexity is present at different spatial scales, but it is especially crucial to take into account at a global scale, as it has a huge impact on the global water cycle (Sheil, 2018), through its interaction with the atmosphere (both inputs and outputs for the continents) and the ocean (outputs for the continental waters). In this context, estimating river's dynamics is critical. It is used for assessing river basin water balance and its storage variability at monthly to multidecadal time scales, for understanding and forecasting flood and drought events, for climate change studies, etc. It is also important information for water managers, as it impacts a wide range of human activities (flood risk, food production, water supply and quality among others (Wood et al., 2011)).

Global estimates of river dynamics, including, discharge (Q), water surface elevation (WSE) and flooded water extent (FWE) however still remains a challenge. A lot of basins in the world remains poorly gauged (Loukas and Vasiliades, 2014; Nijzink et al., 2018) especially in numerous developing countries where ground network is sparse and irregularly distributed. Usually, discharge series relative to a specific gauging station are estimated by converting measured water level into discharge using a rating-curve. Discharge errors associated to such kind of measurements range approximately from 6% to 20% (Clark et al., 2008; Herschy, 2002; Pelletier, 1988; Schmidt, 2002). Monitoring water extent, storage and flow variability in areas with complex channel networks (e.g. braided rivers, wetlands, etc.) are however difficult to monitor with traditional gauges

(Garambois et al., 2019). In addition, it has been noticed that a global decrease in measurements networks during the last decades (Alsdorf et al., 2003, 2007; Gleason et al., 2018; Sivapalan, 2003), and their availability for scientific purposes could be limited due to institutional or international policies, restricting the exchange of data (Alsdorf et al., 2007).

To circumnavegate these limitations, hydrological models could be used to estimate river variability at global and large scales, with less precision than in situ gages. Over the last years, these models' conceptual and physical framework, and computation time have improved, providing more accurate simulation of hydrologic and hydraulic processes at global scale (de Paiva et al., 2013; Gao et al., 2010; Sood and Smakhtin, 2015; Yamazaki et al., 2013). Nevertheless, they still have uncertainties resulting from many sources, such as hydro-meteorological forcing, model structure, model parameters and observation data used to calibrate and validate the model (Döll et al., 2008; Gupta et al., 1998; Kauffeldt et al., 2016; Madsen, 2000; Siqueira et al., 2018; Thielen-Del Pozo et al., 2010; Wanders et al., 2014). Global hydrological models (GHM) could provide estimates of discharge with errors ranging from 52% to 103% (relative root-mean-square errors RRMSE) in South America based on our extended estimates of the comparison between HTESSEL, LISFLOOD and WaterGAP models made by Siqueira et al. (2018). In addition, Fleischmann et al. (2019) evaluated hydrologic-hydrodynamic experiments at different spatial scale. They found that modeled global water level has uncertainties, for the median of the sampled monitoring stations, of 7.4 m and 1.3 m for the absolute value and anomalies, respectively. The water level anomaly was calculated by subtracting the series average from the daily values. As for the discharge, the median of Nash-Sutcliffe (NSE) index and the coefficient of variation reached values of 0.67 and 0.41, respectively.

In this context, collecting complementary observations to in situ measurements is fundamental in helping to improve these hydrological models and to get a finer spatialized estimation of water fluxes at the continent's surfaces (Alsdorf et al., 2007; López et al., 2017). That is why, during recent decades, remote sensing data have been used to provide such type of measurements thanks to their i) greater spatial coverage (Engman, 1995; Tang et al., 2009; van Dijk and Renzullo, 2011; Wanders et al., 2014) and ii) wide range of spatiotemporal, radiometric and spectral resolutions.

Concurrently, data assimilation (DA) techniques have been developed to provide an effective way in which to combine information from models and measurements with an optimum analysis or estimation (Reichle, 2008). Many hydrological models and DA schemes have been widely used for the improvement of the estimations of their state variables using remote sensing observations, such as soil moisture (Baguis and Roulin, 2017; Crow and Ryu, 2008; Massari et al., 2015), terrestrial water storage change (Khaki et al., 2019, 2018), flooded water extent (Lai et al., 2014).

To observe elevation of open waters, multiple nadir radar altimeters missions have also been used in hydrologic studies by the assimilation of water surface elevations (WSE) (Michailovsky et al., 2013; Paiva et al., 2013) or discharge generated by rate curves altimetry based (Emery et al., 2018; Paris et al., 2016). Radar altimeters measure only along their ground track, which can have an intertrack distance at the equator between 300 km and 80 km, missing a large number of continental surface water bodies (Biancamaria et al., 2017; Legresy et al., 2005; Papa et al., 2003). Due to of their nadir measurements, the spatial and temporal resolution of present altimeters cannot fully observe the spatial features of flow wave propagation and flood dynamics for medium to large rivers (David et al., 2011). To overcome this issue and in order to provide 2D observation of WSE, the future wide swath altimetry mission Surface and Ocean

Topography (SWOT; Durand et al., 2010) is currently under development by NASA, CNES (Centre National d'Etudes Spatiales), CSA/ASC (Canadian Space Agency/Agence Spatiale Canadienne), and UKSA (United-Kingdom Space Agency). Its launch is currently scheduled around early 2022. The SWOT mission is planned to make high-resolution measurements of the elevation of land surface water and ocean topography, with a quasi-global coverage between 78°S and 78°N. SWOT is designed, in principle, to be able to observe the seasonality of large portion of river and lakes globally (Biancamaria et al., 2016). SWOT will provide global estimates of WSE and flooded water extent (FWE) with expected accuracy of less than 10 cm and 15 %, respectively, for 1 km^2 areas, i.e. 100m (width) x 10km (long) river reaches (Desai, 2018). In addition, several efforts have been made for estimate discharge from SWOT observations, using various algorithms whose uncertainties can reach, in better cases, 35% for the relative root-mean-squared error (RRMSE) for the daily discharge (Durand et al., 2016). Although observations from SWOT will not be a replacement of in-situ stations (Biancamaria et al., 2016), the assimilation of SWOT measurements into hydrologic models can be an alternative for the improvement of the accuracy of such estimates.

Previous studies developed DA techniques to ingest SWOT synthetic data (hereafter called SWOT-like observations) or observations from AirSWOT (an airborne variant of the SWOT instrument) into hydrodynamic models. Many of these studies mainly aimed to assimilate synthetic water surface elevations. They showed the benefits of improving model parameters (e.g. Pedinotti et al. (2014); Yoon et al. (2012)), state variables (Andreadis et al., 2017, 2007; Biancamaria et al., 2011; Durand et al., 2008; Fisher et al., 2018; Tuozzolo et al., 2019) or both together (e.g. Oubanas et al. (2018a, 2018b)) in which the latter is certainly challenging. Most of them however were applied in a non-multiconnected river network (e.g. Oubanas et al. (2018a, 2018b); Tuozzolo et

al. (2019)) and/or with only a few SWOT-like observations errors, *i.e.* white noise, no correlation of the measurement errors along the swath; usually for studies that have been assessed on a large scale (e.g. Pedinotti et al. (2014); Yang et al. (2019); Yoon et al. (2013)).

SWOT will however provide global measurements of WSE and is therefore particularly well suited for regional to global hydrology models which is why it is important to explore the benefits of SWOT data at the scale of the whole basin river network (and not just in a non-multiconnected river network). In particular, the assimilation of SWOT observations into global hydrological models to correct multiple state variables (WSE, FWE and Q) should be investigated, together with tests of the sensitivity of the assimilation system to different model and observation errors. Currently, only a few works investigated the use of wide swath altimetry WSE, altimetry-based discharge, river storage change or discharge at a basin scale (Emery et al., 2018; Pedinotti et al., 2014; Yang et al., 2019). These studies did not test however the assimilation of different variables altogether (WSE, FWE and Q) and only Yang et al. (2019) used estimates of complex model errors.

The purpose of this paper is therefore to assess the integration of DA from SWOT-like observations into a large-scale hydrologic-hydrodynamic model applied at basin scale. To do so, some experiments have been designed to address the following scientific questions: how can the assimilation of different SWOT-like observations improve global and continental hydrological models? how sensitive is the DA scheme to the uncertainties of the parameters of the model? is the assimilation of multiple variables necessary to further improve large-scale hydrological models? In this way, the aims of this study are: i) to implement and assess the DA of SWOT observations (WSE, FWE and Q) into a hydrologic-hydrodynamic large-scale model, ii) to assess the sensitivity of the model to

different ranges of parameters representative of GHMs' source of errors, and iii) to evaluate multi-variables assimilation compared to single variable assimilation. Therefore, this study will be performed on a large basin (the Purus basin) as a proof-of-concept, and model uncertainties will be set up to be representative of GHM errors.

Section 2 describes the general framework and the design of the SWOT Observing System Simulation Experiment (OSSE), the SWOT mission, the study area, the semi-distributed hydrological-hydrodynamic model and the DA scheme developed in this research. In section 3, the characterization of the sources of errors in models at global scale are delineated. Section 4 presents how SWOT-like observations are generated and section 5 details the setup of the experiments. Section 6 shows the main results and discussions of the following experiments: i) simulations of uncertainty compliant with GHM ones, ii) sensitivity of the model to different scenarios and, iii) the improvements obtained by assimilating SWOT-like data using rather absolute values and their anomalies. Conclusions and perspectives are outlined in Section 7.

2. Design of the SWOT Observing System Simulation Experiment

Figure 1 shows the general framework of this research. In the figure, three main steps are described: "truth" simulation, open loop simulation, and simulation with DA. For the "truth" simulation, which consists of the calibrated version of the model, the superscript *t* is used. This setup is described in detail in section 2.2.2. The water masks from this simulation are used as inputs to the SWOT simulator to generate synthetic SWOT observations, as explained in section 4.2. These observations are then used, via an EnKF method, to update the state variables of the Open-loop simulation. For the open-loop (background) and the updated simulations, the superscripts *f* and *a* are used.

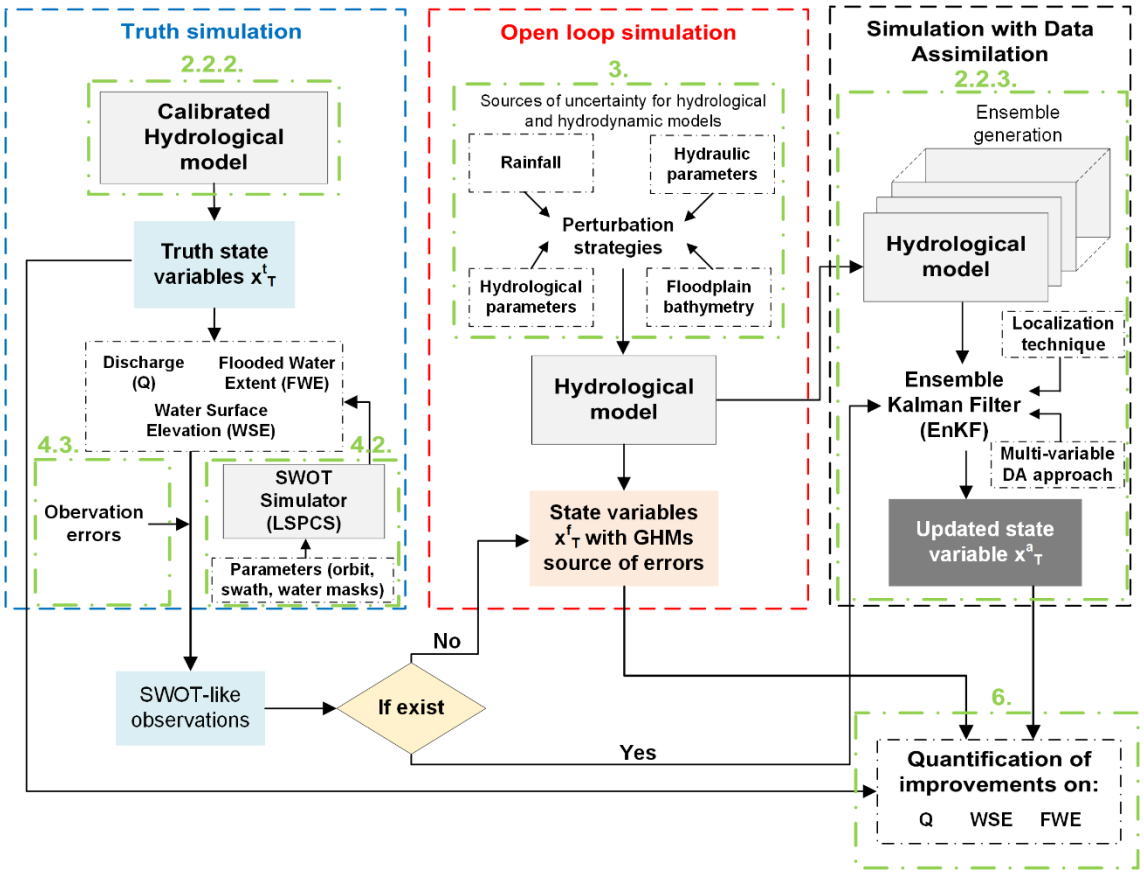

Figure 1. General framework of the Observing System Simulation Experiment, which represents the stages of the simulation within the dotted rectangles for truth (blue), open-loop (red) and assimilation (black). The green dotted rectangles refer to the sections of the manuscript.

2.1. Observing System Simulation Experiment

As SWOT data are currently not yet available, this study is designed as an Observing System Simulation Experiment (OSSE), also known as twin experiment. OSSE are experiments designed to assess how a new observing system might benefit a current model framework. It is done using one model realization considered as the "reference" or "true" state and then some virtual measurements of this reference state by the new observing system are estimated. Finally, these new virtual observations are assimilated in the model, which has been "corrupted" to be representative of the expected model errors. OSSE could therefore assess the potential of the observing system in order

to correct the model outputs or parameters, by comparing the "true" state, the initial one from the "corrupted" model and the one after assimilation of virtual observations. Of course, the results of OSSE are extremely dependent on the level of accuracy of the virtual measurements (i.e. how realistic they are) and the accuracy of the model errors taken into account. Besides, in twin experiments, the same model is used for the reference state and the corrupted state.

OSSE are used to assess the potential of future satellite observations to correct Atmosphere, ocean or hydrology-hydraulic models, as has already been the case for the SWOT mission (see for example Biancamaria et al. (2016a) for a review of such type of study). The current study is in line with such studies. For this OSSE, the hydrologic and hydrodynamic MGB (Modelo de Grandes Bacias) model was used to compute the "truth" and the "corrupted" versions. The corrupted version of the model was notably set up to represent the uncertainties of GHM. The whole Purus basin has been chosen as a case study, despite the fact that coverage gaps can be locally larger in this region (10°S and 10°N) than at mid and high latitudes (Biancamaria et al., 2016). The Purus river represents a large basin with a more complex river network than several previous assessments of SWOT satellite, which mostly used non-multiconnected river networks.

Among the DA methods derived from the Kalman Filter (KF) the EnKF have become popular in the field of hydrology and consequently widely used to combine large-scale hydrological models and remote sensing data (Chen et al., 2013; Clark et al., 2008; Neal et al., 2007; Paiva et al., 2013; Revilla-Romero et al., 2016; Sun et al., 2016). EnKF allows implementing covariance matrix from an ensemble of corrupted model runs and therefore take into account more complex errors than the KF. Therefore, the EnKF DA scheme was chosen in this research to update the state variables of the model by

assimilating synthetic SWOT-like observations. These observations are generated with the SWOT simulator described in section 5.4.

2.2. Case study

2.2.1. The Purus basin

The Purus basin has an extent of ~370,000 km^2 (Fig. 2) and is one of the major tributaries of the Amazon River. The Purus River has a high concentration of suspended sediments, mainly composed by silt and clay that comes from the Andes (McClain and Naiman, 2008), which influences its geomorphology (Latrubesse, 2008). Due to its meandering nature, it has a large river length of ~3,380 km (Goulding et al., 2003). It has high interconnectivity between the main river and floodplains, of the basin containing lakes, unflooded and flooded forests, and floating-meadows. Besides, the river mainstream is affected by backwater effects close to its mouth which is why the Purus basin has large environmental and hydraulic complexity (Meade et al., 1991, Goulding et al., 2003).

The mean annual discharge is estimated to be 9,500 $m^3.s^{-1}$ at Beaba (Cariuacanga) gauge station, near its confluence with the Solimões River. The Purus river main direction is south-west to northeast, with a channel pattern of tortuous meander (Latrubesse, 2008).

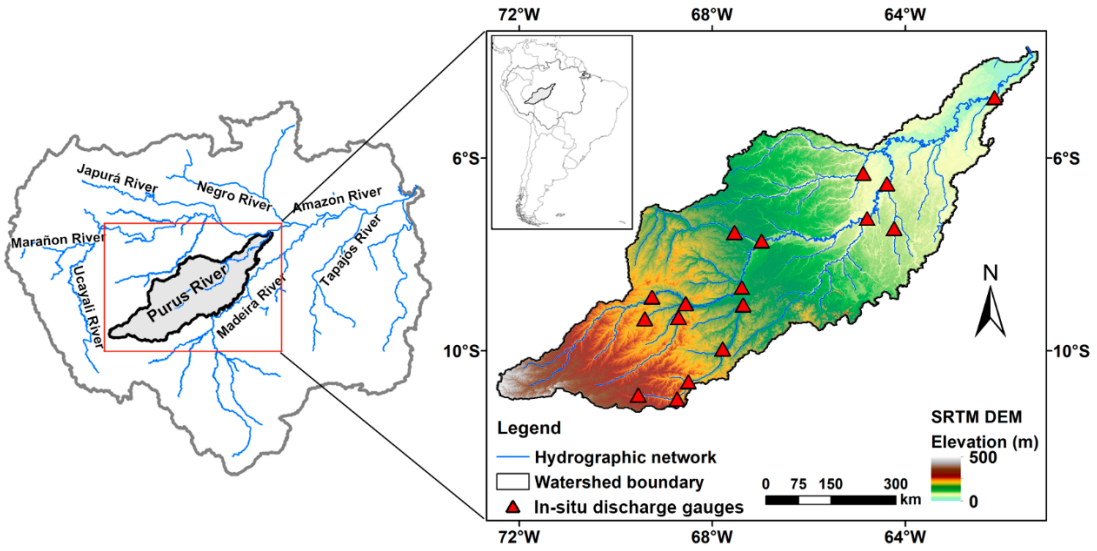

Figure 2. Map of Purus Basin, with in-situ discharge gauges (red triangles). The background image on the right panel corresponds to the digital elevation model of the SRTM.

2.2.2. The hydrologic-hydrodynamic model

In this research we use the large-scale hydrologic-hydrodynamic MGB model. The MGB model was selected due to (i) its satisfactory performance for large-scale applications (e.g., de Paiva et al. (2013); Pontes et al. (2017); Siqueira et al. (2018)), (ii) successful applications in the past in data assimilation (e.g., Paiva et al. (2013); Wongchuig et al. (2019)), which demonstrated the potential of this methodology to improve spatio-temporal estimates of hydraulic variables and (iii) its potential to reach levels of comparison with GHMs, i.e., LISFLOOD, WaterGAP3 and HTESSEL (Siqueira et al., 2018).

The MGB is a semi-distributed hydrological model which uses physical and conceptual based equations to simulate the continental phase of the hydrological cycle (Collischonn et al., 2007). The watershed is discretized into irregular unit-catchments and further into hydrological response units (HRUs), where vertical water and energy budget

are computed individually. For the hydrodynamic component, each unit-catchment is composed by a river reach that includes both channel and floodplain units, the latter depicted as a simple storage with ineffective flow (Pontes et al., 2017; Siqueira et al., 2018). The surface, sub-surface and groundwater runoff produced at each unit-catchment into the hydrologic module are routed to the stream network based on a linear reservoir concept. The main hydrological soil parameters of the model are related to the saturation excess concept based on the variable contributing area concept of the ARNO model (Todini, 1996). The flow routing in river channels is computed using the local inertial method (Bates et al., 2010; Pontes et al., 2017). This is an explicit finite difference approximation of the full 1D Saint-Venant equations by neglecting the convective acceleration term from the momentum equation. It is nonetheless able to represent backwater effects, floodplain attenuation and flood wave transport along rivers in both 1D and 2D dimensions (Getirana et al., 2017; Yamazaki et al., 2013). The main hydraulic state variables which will be related with SWOT-like observations are discharge, water surface elevation and flooded water extent.

Within MGB, the floodplain is represented as storage units without active flow. River and floodplain exchange water instantaneously, and water surface elevation is assumed the same along the river-floodplain system within each unit-catchment (Paiva et al., 2011). Channel cross sections are assumed to be rectangular, as typically adopted in large scale hydraulic modeling (de Paiva et al., 2013; Trigg et al., 2009). Required parameters for the river-floodplain routing are channel bed elevation, cross section bankfull width and depth, and Manning roughness coefficient. The hydrodynamic routing time step is determined by the Courant-Friedrichs-Levy condition with a multiplier parameter for ensuring numerical stability (Bates et al., 2010; Yamazaki et al., 2011).

Detailed information for hydraulic channel-floodplain computation is described in Supplementary material.

The model setup used here over the Purus basin is a resampled application of (Siqueira et al., 2018), which was discretized into 1613 unit-catchments and river reaches of ~10 km. The model was forced using MSWEP v 1.2 precipitation dataset (Beck et al., 2016), with spatial resolution of 0.25° x 0.25° and daily time step for a period spanning 15 years (2000-2015) and monthly meteorological data obtained from the CRU CL 2.0 dataset (New et al., 2002). The model parameters related to soil water budget were calibrated using discharge data from in situ stream gauges (17 stations) and a single set of hydrological parameters for all basins has been established. The hydraulic cross section bankfull width and depth were estimated from geomorphologic equations from Paiva et al. (2011) and the floodplain topography was from Bare Earth digital elevation model upscaled to 500 m spatial resolution (O'Loughlin et al., 2016).

2.2.3. Data assimilation scheme

Among data assimilation techniques, the Ensemble Kalman Filter (EnKF) (Burgers et al., 1998; Evensen, 1994) has become popular due to its relative simple conceptual formulation and computational implementation (Evensen, 2003). The EnKF-based methods have been widely used by the SWOT scientific community such as Andreadis et al. (2007), Durand et al. (2008), Biancamaria et al. (2011), Yoon et al. (2012), Andreadis and Schumann (2014), Munier et al. (2015), Revel et al. (2019), among others. It uses a Monte Carlo formulation based on the concepts of the Kalman Filter (KF). The EnKF method, uses an ensemble of state variables to sample model error and compute covariance error matrix used to estimate the Kalman gain. To achieve this, it is

common to estimate these errors from the perturbation of the model's forcing or parameters (Biancamaria et al., 2011; Liu et al., 2012; Paiva et al., 2013). From the background ensemble the sample mean and error covariances are calculated. During the analysis stage the covariance matrices of the errors from the model and observations are then used to add to the background state vector a correction that corresponds to the so-called Kalman gain apply to the difference between the observation and the background state vector projected into the observation space (Eq. 1 to 3).

The implementation of the EnKF DA scheme in MGB was based on the algorithm developed by Evensen (2004). The main goal of EnKF is the optimization of the variance of the model errors based on model and observation uncertainties to provide a better estimation of the state variables of the model (called the analysis, noted x^a hereafter).

The matrix of the background ensemble of model states x^f, is represented as:

$$\mathbf{x}^f = \left(\mathbf{x}_1^f, \mathbf{x}_2^f, \dots, \mathbf{x}_{N_{ens}}^f\right) \quad (1)$$

where x_i^f represents each ensemble member of the model states until the total number of defined members (N_{ens}).

The analysis x^a is estimated by the EnKF as follows:

$$\mathbf{x}^a = \mathbf{x}^f + \mathbf{K}_e(\boldsymbol{y} - \mathbf{H}\mathbf{x}^f) \quad (2)$$

$$\mathbf{K}_e = \mathbf{P}_e^f \mathbf{H}^T \left[\mathbf{H}\mathbf{P}_e^f \mathbf{H}^T + \mathbf{R}_e\right]^{-1} \quad (3)$$

where x^a is the estimated model state and x^f the background ensemble of model states (Eq. 1), K the Kalman Gain, P^f and R covariance matrices of model (q) and observation (ε) uncertainties, respectively, H is a function that relates the model state variables x^f to its corresponding observation y. The $\left(\boldsymbol{y} - \mathbf{H}\mathbf{x}^f\right)$ expression is also called innovation matrix.

Detailed description about the generation of the covariance matrix of the estate variables of the model ($\mathbf{P}_e^f$) and the observation ($\mathbf{R}_e$) is showed in supplementary material.

Several improvements to the EnKF scheme were made, for instance the Localization Analysis (LA) was proposed by Houtekamer and Mitchell (2001) who use the "covariance localization" method in order to limit the updating of state variable into a spatially area from the observation. It is important to avoid updates due to spurious correlations between two points mainly because i) the use of limited number of ensemble members, mostly to avoid large computational effort and ii) large distant or physically disconnected points, which could have a significant impact in large scale regions. Detailed information is described in supplementary material. To provide improvements on hydrologic-hydrodynamic simulations by the use of SWOT-like observations, a DA scheme from multi-variables was also implemented. For its implementation, specifically three matrices that compose Equations 2 and 3, will increase their dimensions depending on whether on a specific day there is more than one observation. For this study, we assume the simplification that the observations are not correlated with each other.

This multi-variable DA approach, but not necessarily the same mathematics proposed in this paper, has been recently evaluated in hydrology once several remote sensing data are now available; in addition, several authors have realized benefits due to the better representation of more hydrological-hydrodynamic processes (Khaki et al., 2019). In addition, improvements by SWOT using a localization approach for DA already implemented in the MGB by Wongchuig et al. (2019) was assessed as supplementary technique. The multi-variable DA and localization techniques are detailed in the Supplementary material.

3. Modelling Global hydrological model errors

This section describes the generation of the ensemble scenarios of the model by using different sources of error. As stated in section 1, this study aimed to investigate the benefits of assimilating SWOT data into GHMs, as SWOT almost global coverage will be particularly well suited for such type of models. An assessment of typical errors in global and continental models is therefore needed in order to represent uncertainties of models on these scales. The uncertainty on discharge was estimated from the average ensemble of three GHMs. We are assuming that GHMs' errors come primarily from uncertainties on precipitation forcing, river bathymetry, floodplain topography and water balance parameters. An extensive literature review about errors of these parameters in global and continental scales was made, which will be used to corrupt the "truth" model to achieve similar results of uncertainty of GHMs which will be explained later in this section. In addition, the same metrics of errors assessed by Durand et al. (2016) were used in this research to mimic their evaluations on discharge performance, i.e. the RRMSE. The global models assessed were the Land surface model (LSM) HTESSEL coupled offline to CaMa-Flood (Balsamo et al., 2009; Yamazaki et al., 2011), LISFLOOD (Van Der Knijff et al., 2010), WATERGAP (Döll et al., 2009) and the ensemble average of these models (EGHMs). This analysis (Fig. 3) was performed by using 627 in-situ stations of discharge throughout the whole of South America for the period 1990 to 2009. Detailed information about these stations can be found at Siqueira et al. (2018). In this research therefore, the median for RRMSE on discharge (73%, see Fig. 3b) of the EGHMs will be the target of our model set up when all errors are combined.

Figure 3 shows the performance of the assessed GHMs and also the MGB model that was plotted, which showed the best performance among them. These results are similar to Siqueira et al. (2018).

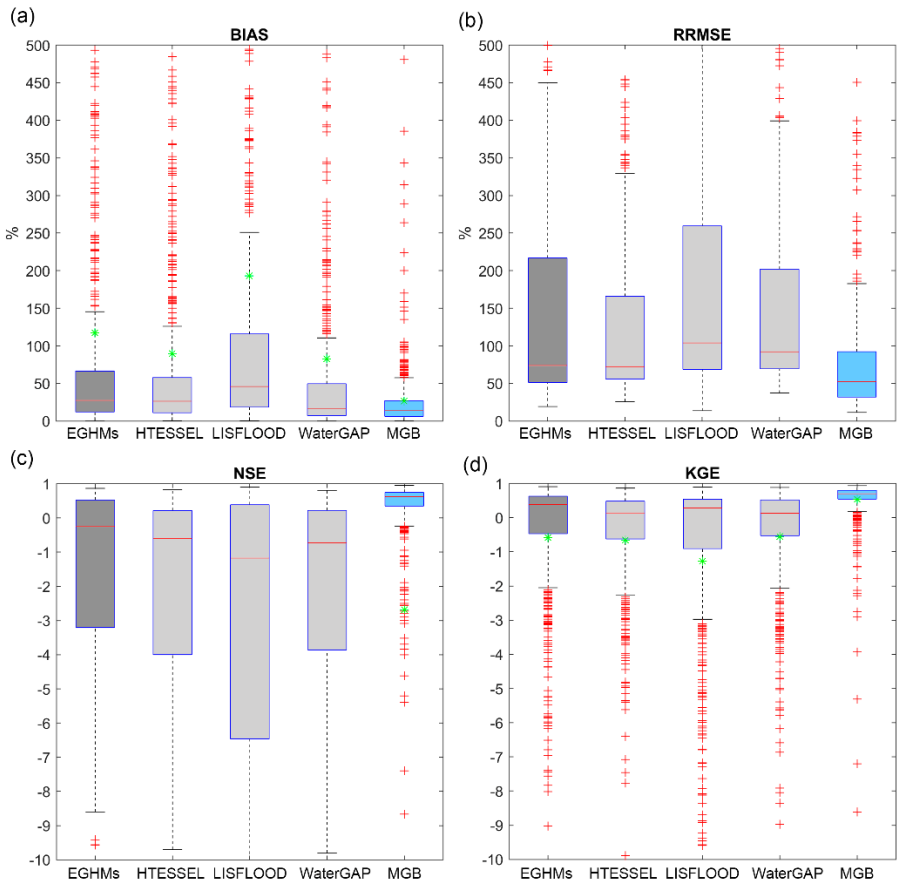

Figure 3. Boxplots of the performance of discharge for global and continental scale hydrological models, showing the ensemble of global models (EGHMs), HTESSEL, LISFLOOD and WaterGAP models and the MGB model.

The performance of EGHMs was chosen as the reference as it represents the best estimator. Hence, the specific RRMSE index was considered to reach errors of discharge for global models, which is around 73% for the median of RRMSE.

See section 1 of the supplementary material where a detailed description of the sources of error used in this study is provided. The main sources of errors (precipitation forcing, hydrological parameters, floodplain bathymetry and hydraulic parameters) of hydrological models were considered in this study, which are schematized in Figure 4 and summarized in Table 1.

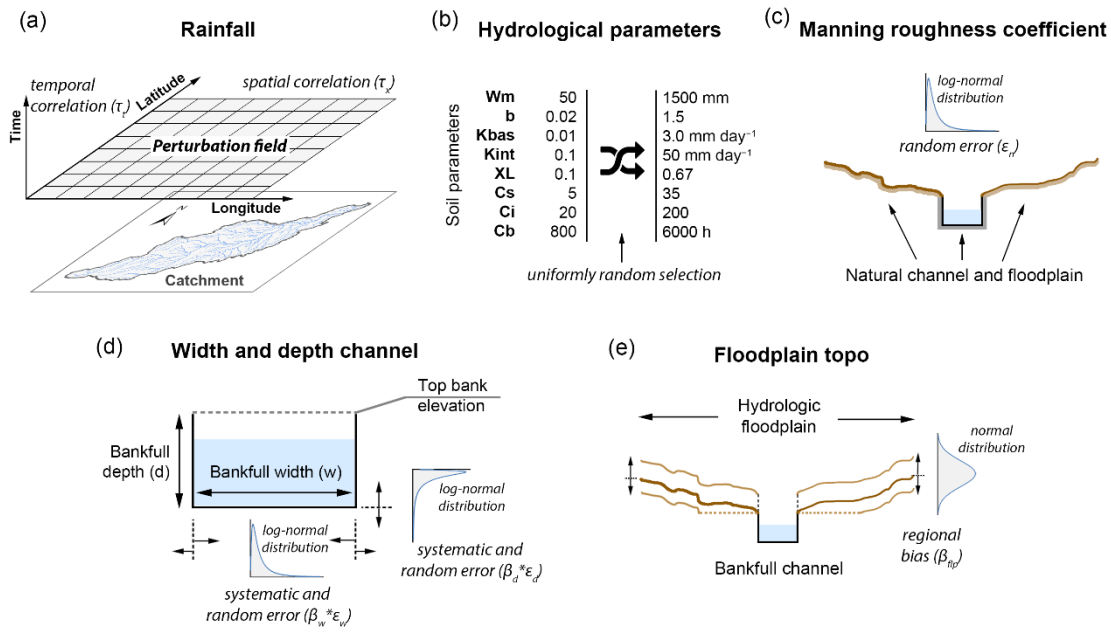

Figure 4. Schematic framework of the perturbation adopted for the model variables. (a) rainfall, (b) hydrological, (c) Manning roughness coefficient, (d) width and depth channel, and (e) floodplain topography.

Systematic (β) and random errors (ε) were mainly considered to perturb the forcing and parameters in this study, once frequently used in water resource assessments (Neppel et al., 2010).

Table 1. Summary of model variables and perturbation setup

	Truth Model	Sources of error Model scenario	Errors	Reference
Rainfall	MSWEP v1.2	Adopted a multiplicative error perturbation	β_p ~logN with relative error of ~25% ε_p ~logN with relative error of ~70%	Nijssen and Lettenmaier (2004), Sun et al. (2018)
Hydrological parameters	Calibrated	Uniform random selection within the parameters' interval	-	Siqueira et al. (2018)
Floodplain Topo (DEM)	SRTM Bare earth	Perturb the hypsometric curve using a regional bias which follows a Gaussian normal distribution. $flp' = flp + \beta_{flp}$	β_{flp} ~N with error of ~10m	Farr et al. (2007), Yamazaki et al. (2017)
Hydraulic parameters (channel width, depth and Manning coefficient)	Geomorphologic equations (Paiva et al., 2011)	$w' = w * \beta_w * \varepsilon_w$ $d' = d * \beta_d * \varepsilon_d$ $n' = n * \varepsilon_n$	β_w and ε_w ~logN (1, 1.12^2) or with relative error of 39% β_b and ε_b~logN (1, 1.22^2) or with relative error of 33% ε_n ~logN (1, 1.69^2) or with relative error of ~50%	Andreadis et al. (2013) Moody and Troutman (2002) Anees et al. (2017)

4. SWOT-like observations

4.1. The SWOT mission

The major payload carried on SWOT satellite is a Ka-band Radar Interferometer (KaRIN), which is a wide swath radar interferometer. The two ground swaths will cover 50 km each, separated by a gap of 20 km (Alsdorf et al., 2007; Biancamaria et al., 2016). To obtain synthetic SWOT data, previous studies (Andreadis et al., 2007; Biancamaria et al., 2011; Durand et al., 2008; Munier et al., 2015; Paiva et al., 2015; Yoon et al., 2013) tested a simple method where spatio-temporal sampling was calculated through SWOT pre-defined orbits and swath tracks and only a white noise was added to the "true" water elevation within the swath tracks in order to simulate SWOT observation errors. Of course, SWOT errors will be much more complex than white noise, some errors will be

correlated along the track, some others across-track and some will even be systematic. These errors could be due to the instrument itself (instrument noise), to the physic of the signal, to some delays due to atmosphere crossing by the electromagnetic wave, to interaction of the electromagnetic signal with the ground (topography effects, interaction with vegetation, water roughness), radar signal processing among others. For a more in-depth review of the SWOT mission error budget, see Fernandez et al. (2017).

4.2. The SWOT simulator

For the past few years, JPL (Jet Propulsion Laboratory) and CNES institutions have developed some SWOT measurements simulators which have been used by the scientific continental hydrology community. The most realistic one the High Resolution (HR) SWOT simulator developed by JPL (Peral et al., 2016) and already used in some previous studies (Bonnema and Hossain, 2019; Bonnema et al., 2016; Chevalier et al., 2019; Domeneghetti et al., 2018; Frasson et al., 2017; Grippa et al., 2019; Langhorst et al., 2019; Oubanas et al., 2018b; Solander et al., 2016), is very difficult to use for large scale applications. It requires high spatial resolution inputs, such as a high-resolution Digital Elevation Model (DEM) with at least 10 meters or higher spatial resolution, along with water elevation maps at the same resolution, which are computationally prohibitive at basin scale. Therefore, the Large Scale Level 2 HR Pixel Cloud Simulator (LSPCS), developed by CNES, was used in this research. This simulator does not explicitly compute the interferogram and its inversion, but rather uses parametrization to compute SWOT-like errors directly for WSE (Desroches et al., 2018). It computes the level 2 SWOT pixel cloud using the SWOT orbit and KaRIn observation geometry and resolution, with some spatially and temporally correlated random noises. It does not take into account layover

error (i.e. error due to the surrounding topography) or error due to the crossing of the atmosphere. Among the main advantages of this simplified version is the less restrictive required inputs (only a water mask is needed) in comparison to the SWOT HR simulator. In addition, it allows a multi temporal simulation relatively easily. Detailed information about LSPCS can be found at (Desroches et al., 2018).

In the Purus river basin, the SWOT-like observation frequency was estimated. For each river reach of 10 km, 97% of the river reaches larger than 50 m will be observed by the satellite and they will be observed between one to three times during each satellite repeat period. The simulation period for LSPCS stretches from September 2011 to September 2012, which covers a flood event (Marengo and Espinoza, 2016).

The SWOT-like observations into the LSPCS were generated in two steps: i) the estimation of the orbits for the study area, and ii) generation of the pixel clouds by using a multitemporal simulation. The calibrated setup of MGB model for the Purus basin was used as the "truth" or "reference" (see section 2). The vectorized water masks of every day, computed from the reference version of MGB, were used as inputs to the LSPCS. SWOT-like observations were estimated from the reference model plus a measurement error from the LSPCS for WSE. The SWOT-like observation is obtained as follows:

$$y = y^t \cdot \varepsilon \tag{4}$$

where $\mathbf{y}$ represents the pseudo-observation (error-containing observation), $\mathbf{y^t}$ the true observation (error-free observation) and ε the error in observations.

For the *WSE*, the mean of the pixel cloud of SWOT *WSE* errors within each catchment were used to perturb the truth *WSE*, and the standard deviation of these errors was assumed as the uncertainty of the *WSE* observation.

In addition, because the SWOT simulator only provides errors on *WSE*, the pseudo-observations of Q and *FWE* corresponded to the same SWOT overpass dates obtained from the *WSE*, and uncertainty is incorporated by a multiplicative noise, which is assumed to follow a log-normal distribution based on errors resulting from analysis of the algorithm uncertainties for Q (Durand et al., 2016) and error budget requirements for *FWE* (Fernandez et al., 2017). The multiplicative noise means that ε (in Eq. 4) is calculated as $(1 + \alpha \cdot r)$ where α represents a specific percentage factor and r a Gaussian-distributed random number with zero mean and standard deviation of 1 (Xue et al., 2007). The specific percentage factor α adds the uncertainty to the dispersion (standard deviation) of the observations.

4.3. Perturbation for the SWOT-like observations

In the EnKF scheme, the innovation matrix $[\mathbf{y} + \epsilon_n - \mathbf{H}\mathbf{x}_n^f]$ is estimated by the difference between the ensemble matrix of perturbed pseudo-observation and the ensemble matrix of state variables ($\mathbf{x}_n^f$) mapped to the measurement space by the **H** operator, while ϵ_n represents an ensemble matrix random noise which follows a Gaussian distribution with mean equal to zero (Evensen, 2003) taking also into account the uncertainties of the observations. The perturbation of each "true" observation is therefore presented in this section, based on different source of uncertainty and model error approaches.

The estimated standard deviation of *WSE* errors in the pixel cloud, provided by LSPCS ($\sigma_{\varepsilon\mathrm{LSPCS}}$), are large. However, some of the errors should decrease while pixels are aggregated (Fernandez et al., 2017). Therefore, pixels were averaged over 1 km^2,

decreasing the error by the square root of the number of pixels aggregated (uncorrelated error), as shown in Equation 5.

$$\varepsilon^{LSPCS} = \frac{\sigma_{\varepsilon^{LSPCS}}}{\sqrt{N}} \quad (5)$$

where $\sigma_{\varepsilon^{LSPCS}}$ is the standard deviation of the sampled pixel clouds and N is the sampled size represented by the number of pixel clouds within 1km^2.

Concerning Q, the multiplicative error is split into two type of errors: a systematic error (ε_{bias}) and a stochastic error (ε_{noise^t}), as shown in Equations 6**¡Error! No se encuentra el origen de la referencia.** and 7. The resulting multiplicative error (ε) is therefore equal to $\varepsilon_{bias} * \varepsilon_{noise^t}$ and corresponds to a log-normal distribution (Table 2), in order to avoid negative discharge. To define the uncertainty of discharge estimation by SWOT, the estimates of the discharge errors by Durand et al. (2016) were used in this research. Here we assume that SWOT-like Q retrievals are as accurate as the most optimistic of these values. We consider that discharge errors are expressed in terms of relative residuals of discharge (RR) which is defined as:

$$RR_t = \frac{Q^{corrupted}{}_t - Q^{true}{}_t}{Q^{true}{}_t} \quad (6)$$

Based on the Equations 4 and 6, the corrupted variable is expressed in terms of RR as following:

$$\varepsilon - 1 = \frac{Q^{corrupted}}{Q^{true}} - 1 \qquad Q^{corrupted} = Q^{true} \cdot (1 + RR) \quad (7)$$

The $(1 + \mathrm{RR})$ is assumed as a log-normal distributed random number, therefore the mean (MRR) and the standard deviation (SDRR) of the discharge relative residual (RR) (Bjerklie et al., 2005; Durand et al., 2016) could be used in the way that:

$$MRR = \frac{1}{N}\sum_{i=1}^{N}\frac{Q^{corrupted}{}_t^{\,i} - Q^{true}{}_t^{\,i}}{Q^{true}{}_t^{\,i}} \qquad mean(1+RR) = 1 + MRR \qquad (8)$$

$$SDRR = \sqrt{\frac{1}{N}\sum_{i=1}^{N}\left(\frac{Q^{corrupted}{}_t^{\,i} - Q^{true}{}_t^{\,i}}{Q^{true}{}_t^{\,i}} - MRR\right)^2} \qquad std(1+RR) = SDRR \qquad (9)$$

These values were already estimated by Baratelli et al. (2018) from Durand et al. (2016) who considered values around -18.8% and 15% as the median of MRR and SDRR respectively for all river algorithms.

Lastly, for *FWE* perturbation only a random noise ($\varepsilon_{noise}^{FWE}{}_t$) was added to the truth. For this purpose, the value of 15% of uncertainty established in the SWOT scientific requirements document (Fernandez et al., 2017) was used. The schematic representation of this section is shown in Figure 5.

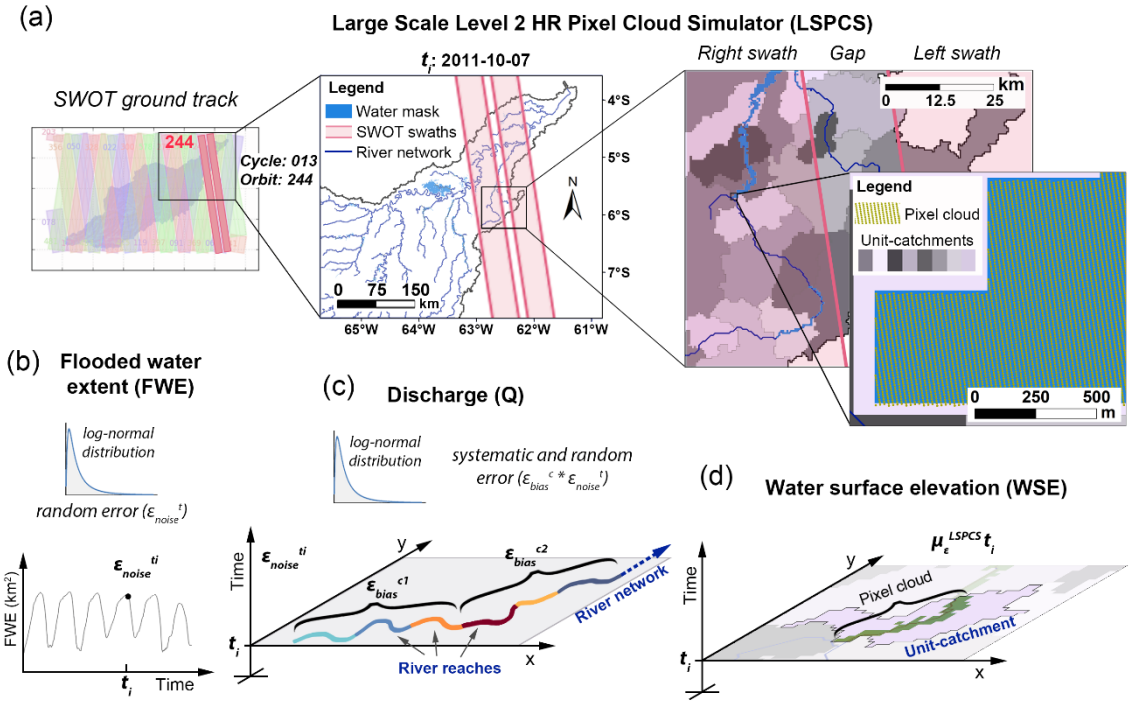

Figure 5. Schematic framework of the (a) Large Scale Level 2 HR Pixel Cloud Simulator (LSPCS) for specific day t_i and the adopted perturbation to generate the SWOT-like observations for (b) Flooded Water Extent (FWE), (c) Discharge (Q), and (d) Water Surface Elevation (WSE).

Table 2. Summarize of the perturbation setup for SWOT-like observations

SWOT-like observation	Uncertainty (assimilation / corruption)		Perturbed model by measurement errors (Gaussian distribution)	# of realizations
WSE	ε^{LSPCS}	min ~0.10 m for 1km^2	$WSE^{corrupted} = WSE^{true} + \mu_{\varepsilon\text{LSPCS}}$	One
Q	Algorithm's uncertainties, (Baratelli et al., 2018; Durand et al., 2016)	MRR and SDRR -18.8% and 15%	$Q^{corrupted} = Q^{true} * \varepsilon_{bias}^{Q\ c} * \varepsilon_{noise^t}^{Q}$	25
FWE	Mission performance and error budget reference (Fernandez et al., 2017).	σ_{FWE} 15 %	$FWE^{corrupted} = FWE^{true} * \varepsilon_{noise^t}^{FWE}$	25

In this study true variables (Q and FWE) are assumed to be corrupted at all-time steps by the random errors of the error terms ($\varepsilon_{noise^t}^{Q}$ and $\varepsilon_{noise^t}^{FWE}$), while the systematic error (ε_{bias}^{Q}) for Q is constant in time and spatially correlated between contiguous catchments within the river network to ensure continuity.

$$\varepsilon_{bias}^{Q} \sim logN\left(1, e^{MRR^2}\right) \quad \varepsilon_{noise^t}^{Q} \sim logN\left(1, e^{SDRR^2}\right) \tag{10}$$

$$\varepsilon_{noise^t}^{FWE} \sim logN\left(1, e^{\sigma_{FWE}{}^2}\right) \tag{11}$$

The continuity assumption for discharge is an important issue for some algorithms tested by Durand et al. (2016) (e.g. AMHG and MetroMan). To ensure that, three contiguous reaches within the river network were considered as **fully spatially correlated**, which means that the same perturbation is used for each cluster of reaches (e.g. group of three reaches). To generate the random numbers by a **multivariate normal distribution**, the following equation was used here:

$$\varepsilon_{bias}^{Q\ \ c} = \rho \cdot \varepsilon_{bias}^{Q\ \ 1} + \sqrt{1-\rho^2} \cdot \varepsilon_{bias}^{Q\ \ 2} \quad (12)$$

where $\varepsilon_{bias}^{Q\ \ 1}$ and $\varepsilon_{bias}^{Q\ \ 2}$ are independent realizations and ρ is the correlation matrix of one and zero, where one represents full correlation.

5. Experiments setting

Table 3 summarizes the experiments defined in this research, where different scenarios are assumed to assess the improvements in the states variables of the model using DA scheme and complementary localization and multi-variable techniques. The observations that will be used in the experiments are Q, WSE, FWE and all the three together (MV), also the anomalies of each one of these variables will be used, defined with the symbol (’). The anomalies were estimated by removing the time averaged values (from both, open-loop and SWOT-like observations) neglecting the first year (2000) that corresponds to the warm up period for the hydrological model, hence bias on the observations would be avoided.

Table 3. Summary of the experiments and main characteristics and setup

Experiment	Assimilated SWOT-like observation *	To assess:	Realizations
1	-	To achieve the uncertainties of GHMs by perturbing forcing and parameters of the model	25
2	WSE, FWE, Q and MV	Sensitivity based on individual and full-combined scenarios of the model from different source of errors	25
3	WSE’, FWE’ and Q’	Improving by assimilating the anomaly of the SWOT-like observations	25

* WSE=Water Surface Elevation, FWE=Flooded Water Extent, Q=Discharge, MV=Multi-variable, “ ’ ” represents the variable’s anomaly

In addition, a localization approach was implemented to estimate the optimal radius of influence in the Purus Basin and to assess the improvements by using this technique. Due to the computational demand, it was only assessed by assimilating WSE. The improvements on RRMSE by using a localization method (Wongchuig et al., 2019) reaches up to ~60% in comparison with no-localization assessing. Enhancements were greater especially for smallest ensemble size (10 – 50) and for a radius of influence of 500 km. Detailed results are shown in the supplementary material section.

The forcing and parameters of the model were disturbed through perturbation strategies described in section 3 to obtain errors similar to GHM errors. For a better representation of uncertainties, 25 realizations were performed for each source of model errors.

Table 4 shows the experiments designed to assess the potential of the assimilation of different variables SWOT observables to correct GHM and assess assimilation results sensitivity to model errors. As shown in Table 4, assimilation results are assessed separately for each source of model error and then with all model errors included, which corresponds to EGHM performance estimated in section three. A reference setup (truth) is therefore compared with 25 realizations of both corrupted scenarios and pseudo-observations. No localization method approach is shown in the main document and the results of the localization approach are shown in the supplementary material.

The main goal of the last part of the experiments is to improve the state variables of the model by assimilating the anomalies of the SWOT-like observations.

Table 4. Summary of the perturbed variables taken into account for the corrupted models regarding the experiments.

SWOT-like obs	Model errors					
	Rainfall	Hydrologic parameters	Floodplain parameters	Hydraulic parameters		
				Depth	Width	Manning
WSE / FWE / Q	x					
		x				
			x			
				x	x	x
	x	x	x	x	x	x
WSE + FWE + Q (MV)	x	x	x	x	x	x
WSE' / FWE' / Q'	x	x	x	x	x	x
WSE' + FWE' + Q' (MV')	x	x	x	x	x	x

* + means the multi-variable assimilation approach, " ' " represents the variable's anomaly

The performance of the simulations has been evaluated by the difference in the relative root mean square error (ΔRRMSE), calculated for each updated state variable i.e. water level, discharge and flooded water extent. The root mean square error is calculated as follows:

$$RRMSE = \sqrt{\frac{\sum_{i=1}^{N}\left(\frac{S_i - T_i}{T_i}\right)^2}{N}} \tag{13}$$

$$\Delta RRMSE = \frac{RRMSE_{assimilation} - RRMSE_{open-loop}}{RRMSE_{open-loop}} \tag{14}$$

where N is the number of days of the windows simulations, S represents the simulation (i.e. Open Loop, DA EnKF), T represents the true model. The $\Delta RRMSE$ compares (relatively) the performance (decreasing of errors) of the model simulation using the DA scheme with respect to the open-loop (free run simulation).

We also used the same metrics by Durand et al. (2016) based on the relative residuals, the equational demonstration of which is shown in supplementary material:

$$RRMSE^2 = MRR^2 + SDRR^2 \quad (15)$$

6. Results and discussions

6.1. Model uncertainties and their sensitivity to different sources of errors

Figure 6 shows the model discharge RRMSE versus the considered source of errors. As found in previous studies (e.g. Clark et al. (2008)), rainfall is the most sensitive parameter in our evaluation. Besides, the full-sources error model achieves a median of RRMSE of 64%. It can be considered representative of GHMs uncertainties, as it is similar to the value of 73% that was found in section 3.

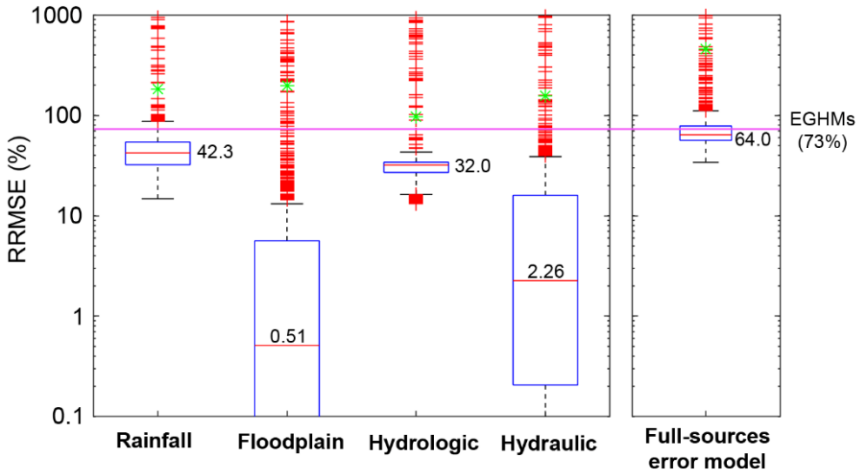

Figure 6. Boxplot in semi-log scale of RRMSE of discharge for the model scenario due to each independent source of error, and for the full-sources error one. Magenta line represents RRMSE value for the ensemble of GHMs. Green dots represent the mean values.

For the scenario which only considers the floodplain as a source of error, the errors were lower than other parameters, which can be explained due to the fact that most parts

of the basin are not inundated during the year, therefore the lower basin region is the most sensitive to this parameter.

In addition, Figures 7a and 7b show the RMSE and RRMSE for FWE, respectively. The errors are greater when rainfall or hydraulic parameter uncertainties are considered. These results can be explained by the strong influence of hydraulic parameters on both WSE and FWE. Fleischmann et al. (2019) found a median EGHM RMSE value for WSE of ~7.4m, on a global scale. This value is higher than the estimates reached here (~4.16 m). This difference is due to the fact that Fleischmann et al. (2019) made a global study, while in our study we are considering "only" the Purus basin. Fleischmann et al. (2019) covers a large range of slopes, which could have abrupt changes in riverbed elevations, leading to significant uncertainties. These cases are not present in the Purus basin.

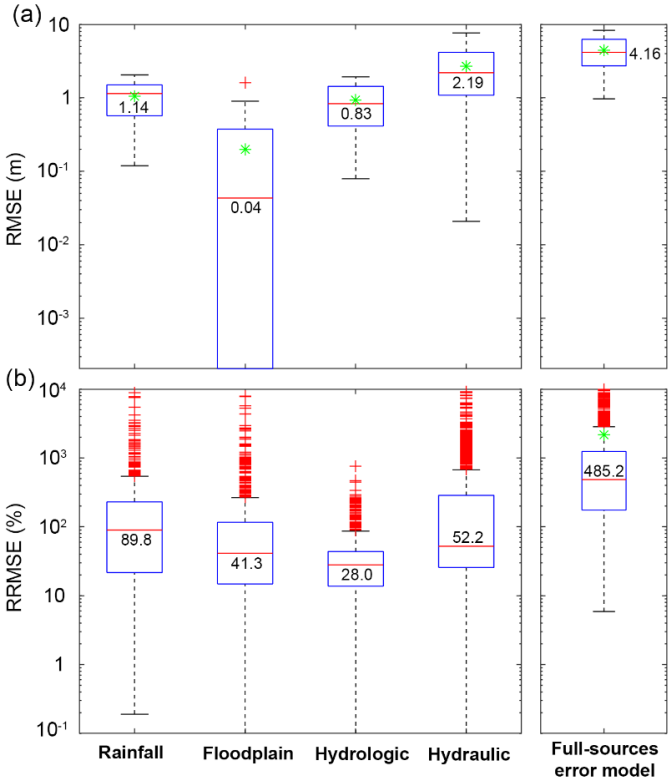

Figure 7. Boxplot in semi-log scale of (a) RMSE of water surface elevation and (b) RRMSE of flooded water extent for the model scenario due to each independent source of error, and for the full-sources error one. Green dots represent the mean values.

The spatial influence of rainfall, floodplain, hydrological and hydraulic errors on the estimates of Q, WSE and FWE is shown in Figure 8. Considering discharge (Q), RRMSE obtained after disruption of rainfall or hydrologic parameters are mainly in the range 10% to 50% for the whole basin. Although few catchments located in the main stem are prone to have the largest errors, this occurs probably due to the aggregation of errors from upstream to downstream, which is also happening for WSE. For the FWE variable, higher RRMSE values are mainly located in the lower part of the basin, which is flatter than upstream and holds a large part of the Purus' floodplains, especially the Piagaçu-Purus Sustainable Development Reserve (approximately 8,342.45 km^2), 40% of which is periodically flooded (Albernaz and Venticinque, 2003).

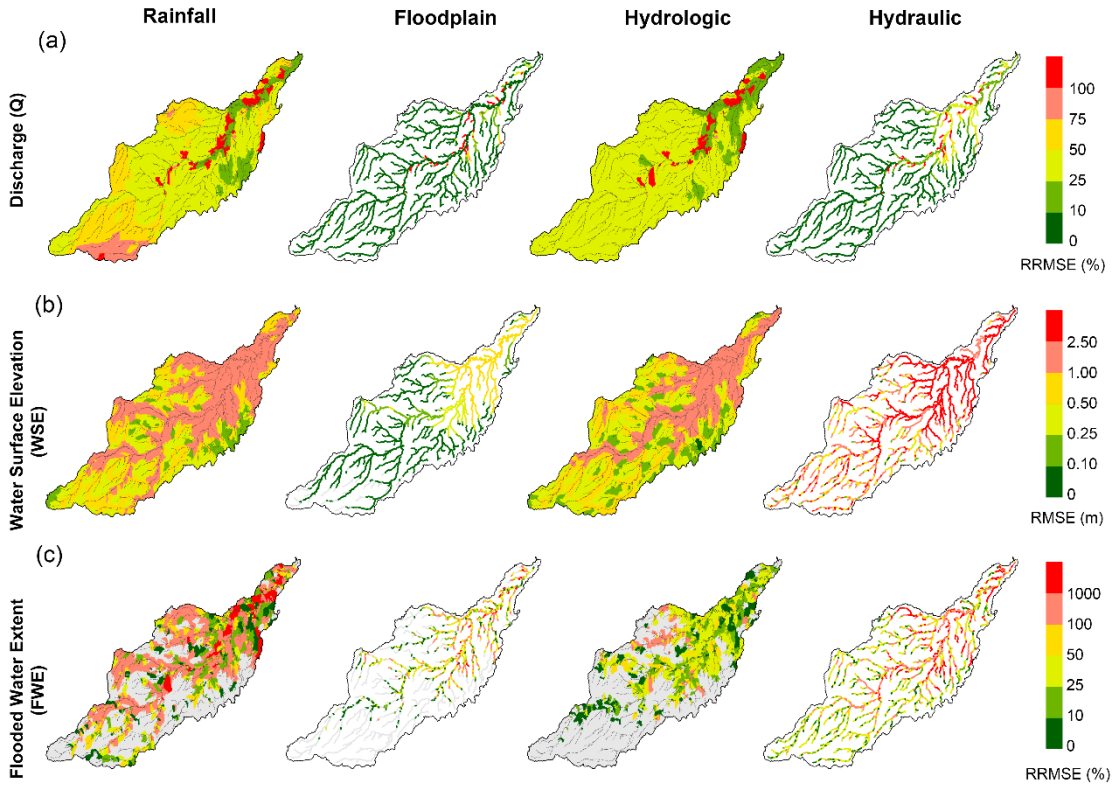

Figure 8. Spatial distribution of the RRMSE of (a) Q, (b) WSE and (c) FWE when the rainfall, floodplain, hydrologic and hydraulic parameters are perturbed. For rainfall and hydrologic color of catchments' area are filled, while for floodplain and hydraulic only river reaches are colored. Gray color means not sensitive.

6.2. Assimilation sensitivity to different sources of errors

Figure 9 shows the reduction of RRMSE for WSE, FWE and Q versus error sources, when independent SWOT-like observations are assimilated.

In general, the assimilation of WSE improves all other variables but with lower improvements for the FWE when the floodplain topography is the source of model errors. It could be due to the strong relationship between the floodplain and water level, depicted in the hypsometric curve that was perturbed. In addition, for the median any improvement was realized for Q when hydraulic parameters were the source of errors, maybe due to the direct relation of width, depth and Manning coefficient on discharge.

Besides, the assimilation of FWE in all the versions of the model with sources of error shows improvements only for the same state variable (FWE). The worst impact was however realized for Q where performance was degraded when rainfall, floodplain and hydraulic scenarios were the source of errors. Finally, the assimilation of Q improved all scenarios for all state variables, although the worst improvements were found when hydraulic parameters were the sources of errors for the other variables (WSE and FWE) only.

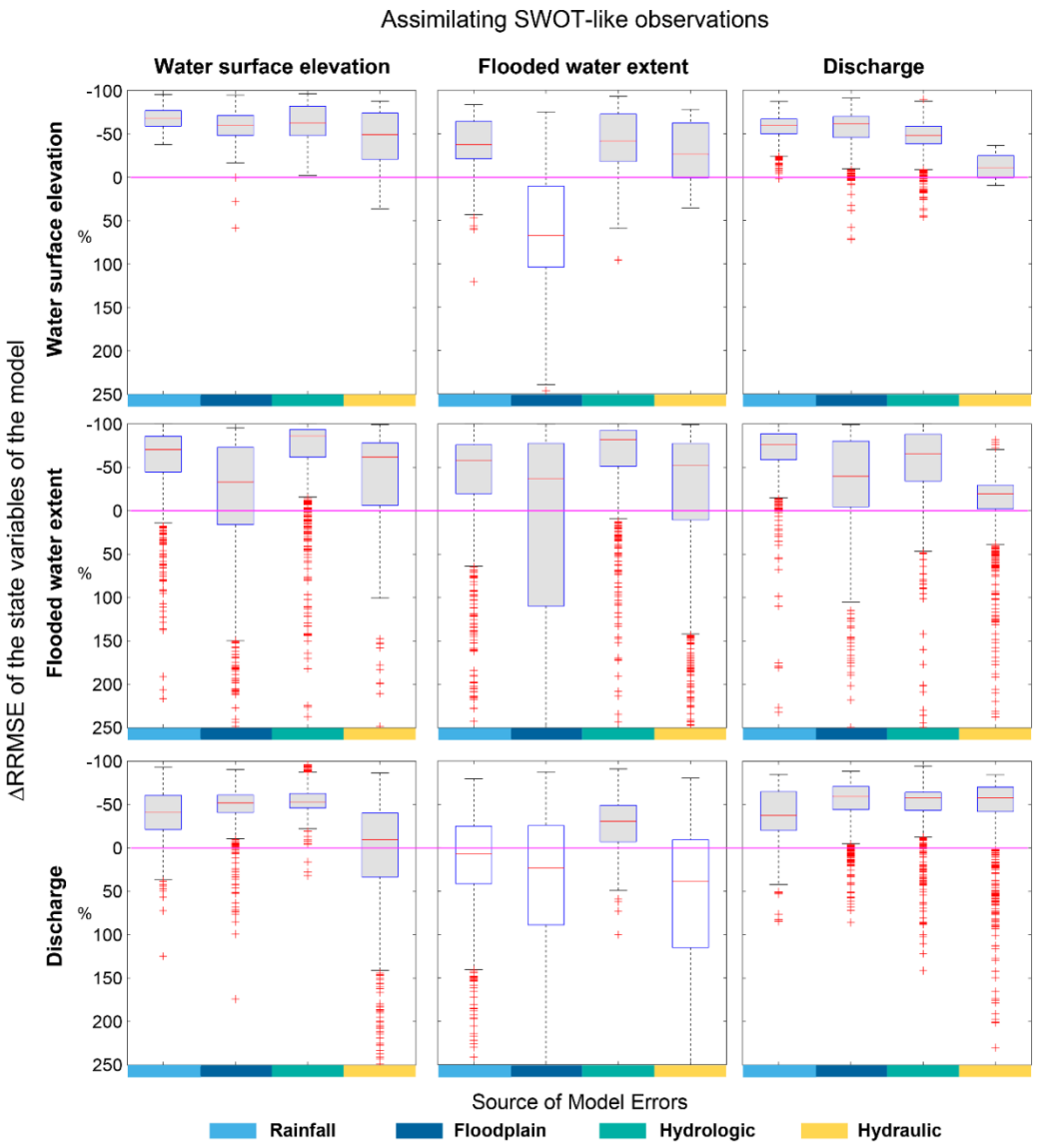

Figure 9. Boxplot of reduction of RRMSE for WSE, FWE and Q for different scenarios of sources of model errors by assimilating correspondent SWOT-like observations. Gray boxes mean improvements on the median of catchments.

From these first results, the following conclusions could be drawn considering the assimilation sensitivity to the state variables regarding all the model's scenarios:

1. Assimilating WSE clearly improves all variables and for all the model sources of errors. It shows however worse improvements in Q when the model assumes the

hydraulic parameter as a source of error, which could be explained by the strong relation between these parameters and Q and WSE estimates.

2. When FWE is assimilated, only FWE is improved for all model errors scenarios. FWE assimilation degrades WSE estimates when the floodplain was the source of error. For Q the aggravation is shown for all scenarios except when hydrologic parameters were the source of errors, likely due to the poor relationship with the hydrodynamic processes.
3. Finally, the assimilation of Q improves all variables and all scenarios. Lower improvements are shown for WSE and FWE when hydraulic parameters are the source of errors. Here we have to emphasize that we are considering an optimistic scenario of the uncertainties of SWOT-like Q, therefore improvements in the performance of the state variables of the model could certainly be overestimated.

6.3. Improvements on performance on a continental and global scale

In this section, all sources of errors are combined to obtain realistic uncertainties, close to GHM ones. Improvements in RRMSE are showed in Figure 10. In general, better performance of the DA framework is obtained for the state variable that is assimilated (e.g. discharge when Q is assimilated). Overall, assimilation of all observations are decreasing RRME, except for WSE, which degrades discharge estimation. This is likely related to errors due to hydraulic parameter, as described in section 6.2. This case shows the importance of improving hydraulic parameters as shown by (Brêda et al.(2019), before assimilating WSE to estimate discharge.

Q is degraded when FWE is assimilated. This result was expected given the sensitivity tests concerning FWE assimilation shown in Figure 9. As described in section

6.1, sources of errors that are physically more related to the estimation of discharge in the MGB model shows more sensitivity in the lower and main stem region. These results demonstrate that, in principle, EnKF has the ability to get close to the true model's variables even in cases of large errors, like those of GHMs. This is however not always the case as shown in Figure 10b.

Results obtained when multiple-variables (MV) are assimilated are shown in Figure 10d. Assimilating all variables allowed improving WSE, Q and FWE. The improvement for each variable is however not as good as the result obtained when only this variable is assimilated.

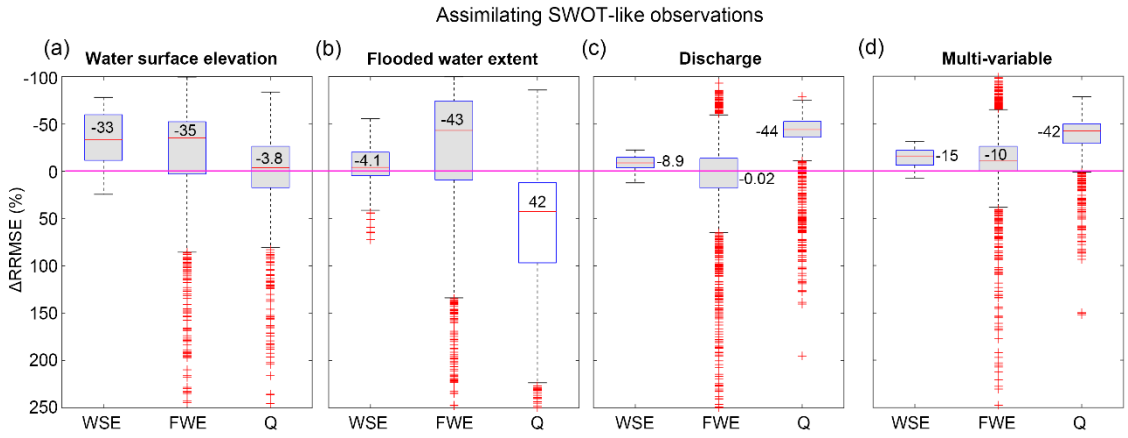

Figure 10. Boxplot of reduction of RRMSE index for WSE, FWE and Q for the model's scenario with full-sources of errors by assimilating correspondent (a-c) SWOT-like observations and (d) MV approach. Gray boxes mean improvements on the median of catchments.

Table 5 sums up the results shown on Figure 10. These results can be compared to previous studies findings. Wongchuig et al. (2019) assimilated in situ observation, which lead to an error decrease that ranges from ~15% to ~20% for a period of ~100 years. Emery et al. (2018) reached an averaged improvement of ~21% by assimilating altimetry-based (ENVISAT) discharge. In contrast, in our assessment over the Purus

basin, assimilating synthetic SWOT observations leads to RRMSE decrease two times greater (~44%) than these previous studies. This can be explained by larger uncertainties in our model setup (that mimics GHMs uncertainties), leading to greater errors decrease, even when uncertainties of SWOT-like discharge (~24%) are greater than in-situ discharge observations (~15%). Indeed, reductions in relative errors may seem large, but in absolute terms this decrease ranges from median values for RRMSE of ~64% (open-loop) to ~36% (DA), which could still be considered large errors for discharge estimation.

Table 5. Values of median of improvements in RRMSE for all catchments when assimilating SWOT-like observations individually and all together.

	SWOT-like observations			
	WSE	**FWE**	**Q**	**MV**
WSE	-33.59	-4.09	-8.88	-15.83
FWE	-35.31	-43.25	**-0.02**	**-10.44**
Q	**-3.84**	**42.53**	-44.15	-42.29

* Values in bold indicate less performance for each column

Finally, Figure 11 shows the spatial distribution of RRMSE reduction. Q is the most challenging state variable to improve, due to the high sensitivity to the hydraulic parameters and floodplain topography. In addition, initial uncertainty of Q could be also influencing their performance. When assimilating WSE or FWE, Q is improved only in the lower part of the main stem where the impact of hydraulic parameter is more sensitive (see section 6.1) than in the upper part of the basin. On the contrary, WSE and FWE variables have a relatively homogeneous sensitivity to hydraulic parameters across the whole of the basin and can therefore be more homogeneously corrected in space, whatever the observed variable assimilated.

It is also quite clear that the use of multi-variable DA could overcome these issues, even when high uncertainties were considered. It should be noted however that RRMSE

patterns when Q is assimilated or when multiple variables are assimilated are quite similar, showing the importance of Q even when multiple variables are assimilated.

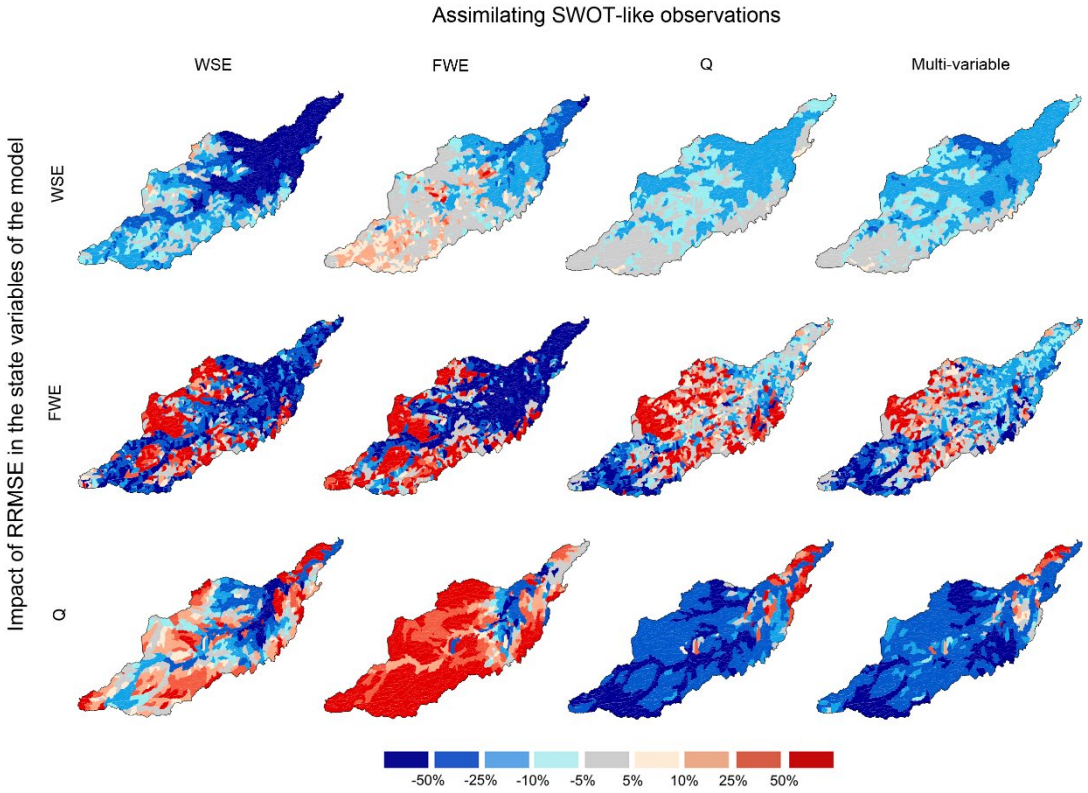

Figure 11. Maps of spatial distribution of the reduction on RRMSE by assimilating absolute values of SWOT-like observations, represented on the blue-red color scale.

With the background and observation errors assumed therefore in this study, SWOT observations of WSE, FWE, and derived Q could be beneficial to correct global and continental scales models outputs. It should be recalled however that when only FWE is assimilated, Q could be quite degraded. Conversely, Q is a large integrative variable that could help to overcome errors even on parameters. In general, SWOT-like information seems useful for hydrological and hydrodynamic assessments, mainly when WSE, Q or multi-variable DA is performed.

To show the aggregation from the full-sources of error model to the SWOT-like observation, the hydrographs and water level series for some locations are also shown in Figures 12 and 13, respectively. These figures show the performance in a specific state variable (Q and WSE) when the same SWOT-like variable is assimilated.

The reduction of uncertainties is clearly shown by DA scheme (gray envelope) during the presence of SWOT-like observations from October 2011 to October 2012. For Q time series, the SWOT-like observations are shown as blue dots that correspond to those belonging to their envelope border.

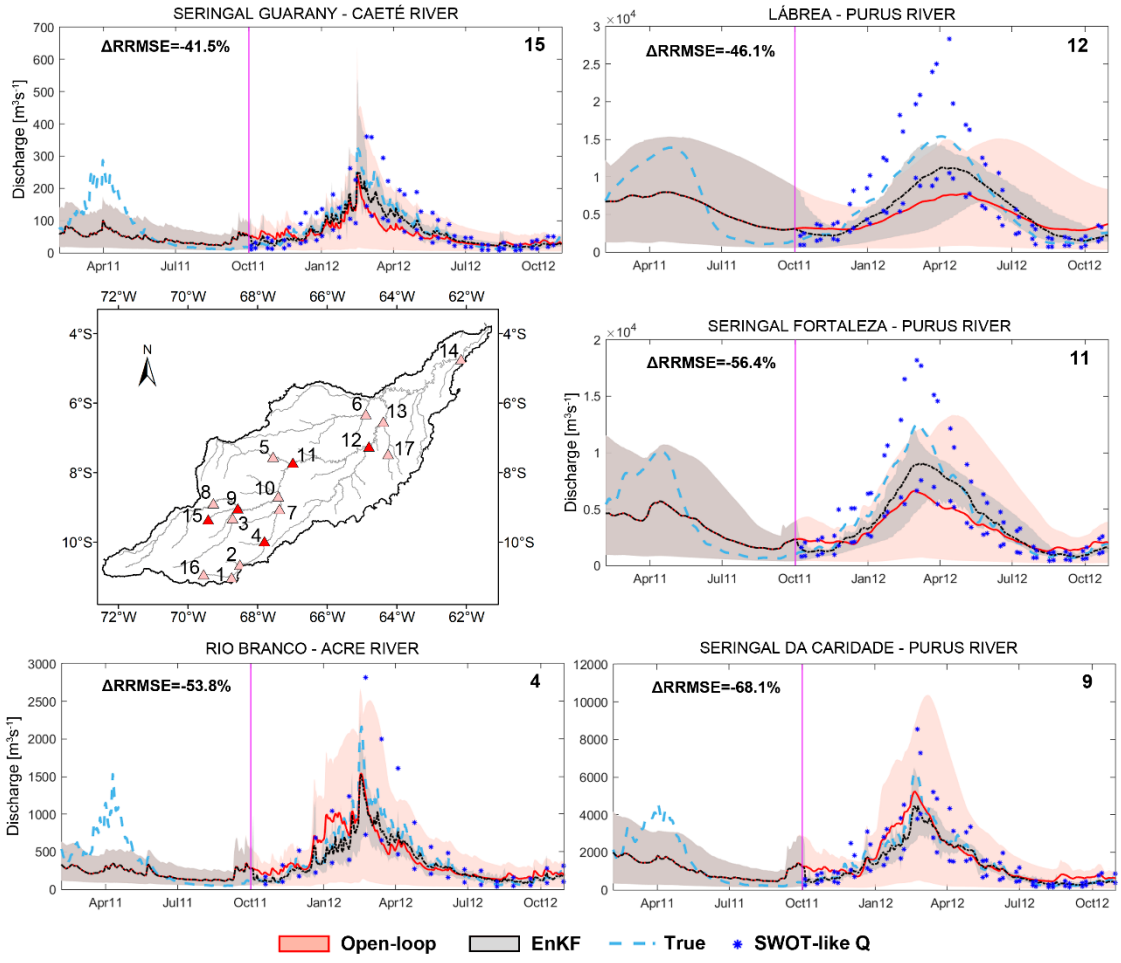

Figure 12. Hydrographs for a few sites at main stem and tributaries when Q is assimilated. The spread of the full-sources error model and the assimilated are represented by red and gray envelopes respectively. Red and black lines represent the mean of the spread of the Open-loop

and of the EnKF simulations respectively. The true model is represented in sky blue dotted lines, and the boundary of the envelope of SWOT-like are represented by the blue dots. Magenta line represents the beginning of the DA performance.

In the case of the time series of water level (Fig. 12), the SWOT-like observations are shown as the only realization coming from the LSPCS. These are close to the truth due to high accuracy. The uncertainties were also reduced by DA scheme (gray envelope) from the Open-loop (red envelope). Some noise was showed by the DA series mainly in tributary rivers where less accuracy was likely found.

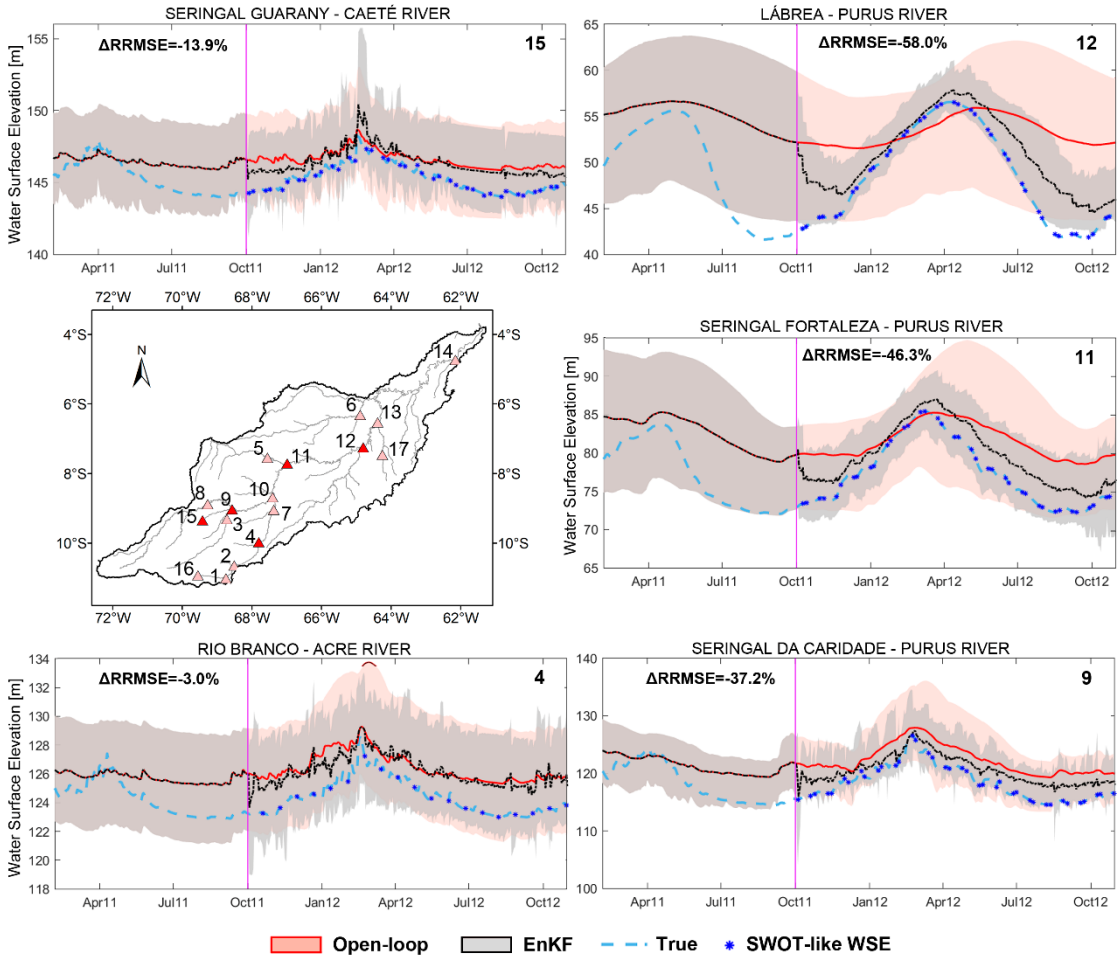

Figure 13. Time series of water level for a few sites at main stem and tributaries, when WSE is assimilated. The spread of the full-sources error model and the assimilated are represented by red and gray envelopes respectively. Red and black lines represent the mean of the spread of the Open-loop and of the EnKF simulations respectively. The true model is represented in sky blue

dotted lines, and the SWOT-like are represented by the blue dots. Magenta line represents the beginning of the DA performance.

6.4. Performance by assimilating anomalies of SWOT-like observations

In this section the performance of the improvements in RRMSE by assimilating SWOT-like anomalies is shown. All sources of model errors are used for this experiment. Figure 14a shows that best performances in the state variables were achieved by assimilating correspondent anomalies of SWOT-like observations, as for experiments in section 6.3. Assimilating WSE anomalies (referred to as WSE' hereafter) leads, in general, to greater reduction of RRMSE than when WSE is assimilated, especially for Q. Besides the performance by assimilating FWE and Q anomalies (referred to as FWE' and Q', respectively, hereafter) clearly presents improvements in the other estate variables contrarily to the results obtained when absolute values are used (FWE and Q). It is due to the fact that anomalies do not have the bias present in the absolute values, especially for Q, for which the bias corresponds to ~18%. This bias corresponds to the MRR described in Section 4, while FWE was only corrupted with a random noise. Finally, assimilation of multi-variable anomalies (noted MV') was also performed and shown in Figure 14d, where similar results were achieved for WSE and FWE than the ones using absolute values. However, Q is lees reduced (ΔRRMSE=-7%) with anomalies, than with absolute values (ΔRRMSE=-42%).

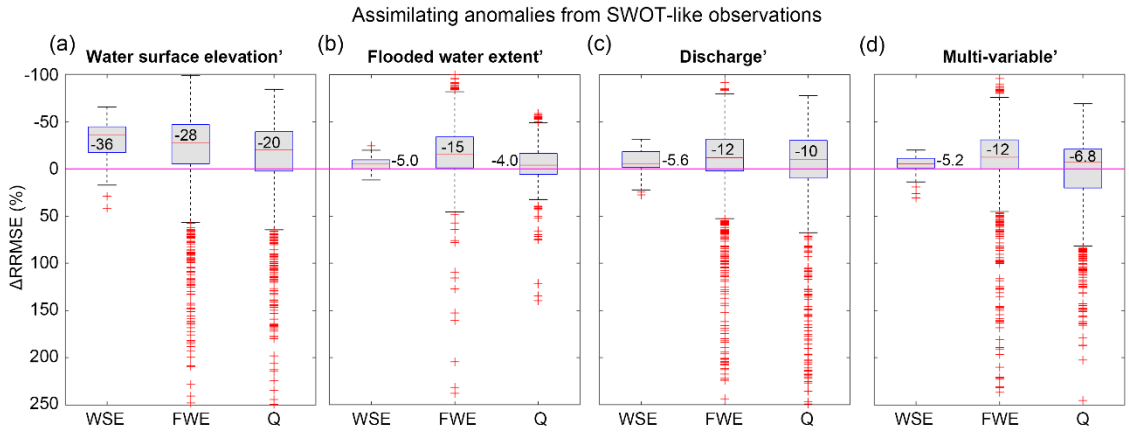

Figure 14. Boxplot of reduction of RRMSE index for WSE, FWE and Q for the full-sources error model version by assimilating correspondent anomalies of (a-c) SWOT-like observations and (d) MV' approach. Gray boxes mean improvements on the median of catchments.

Figure 15 shows the spatial distribution of improvements in RRMSE by assimilating anomalies. Clearly, the assimilation of WSE' further improves the performance of WSE and Q than when absolute values where assimilated. Assimilating WSE' is therefore recommended for GHMs instead of only WSE, at least with this assimilation set up. Besides, the assimilation of FWE' and Q' improved all state variables although it fared slightly better on average than the assimilation of absolute values. Contrarily to absolute value, the pattern of RRMSE between Q' and MV' is not the same. Finally, in general the assimilation of anomalies can improve results due to the removal of the bias in SWOT-like observations. If the bias between the observations and the open-loop simulation is large, the improvements can prove larger by using the assimilation of anomalies, once the open-loop simulations represent uncertainties of GHMs.

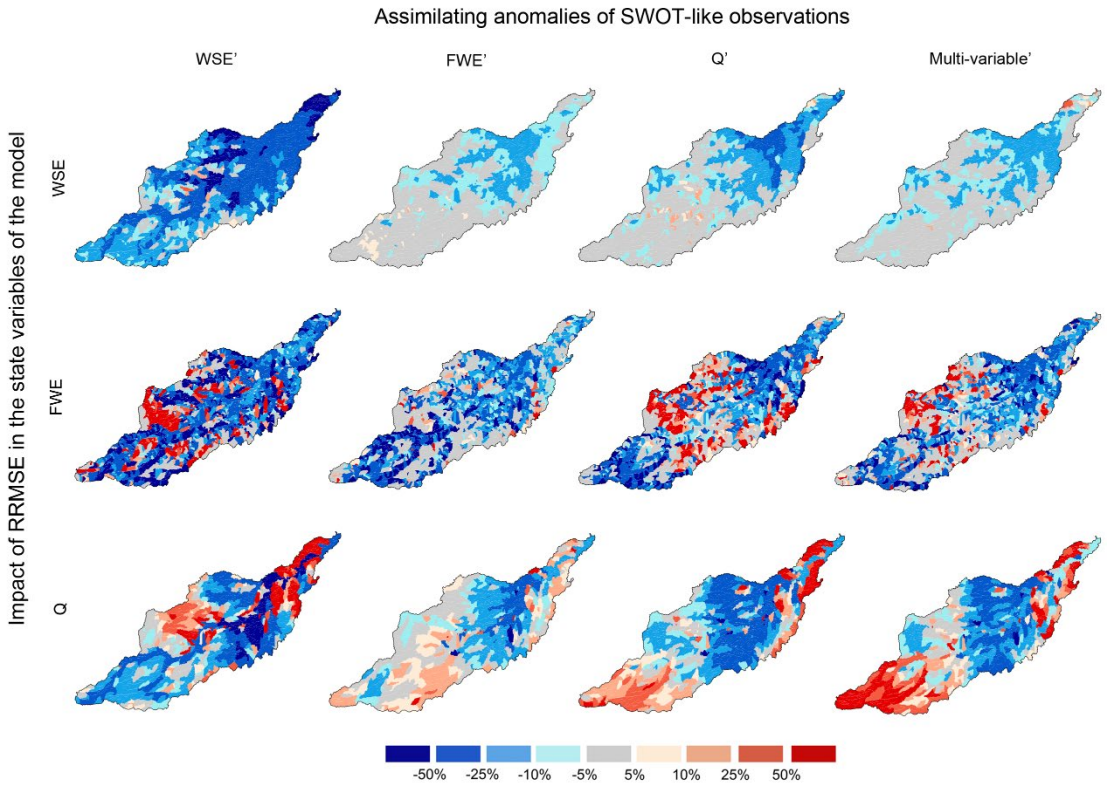

Figure 15. Maps of spatial distribution of the reduction on RRMSE by assimilating anomalies of SWOT-like observations, represented on the blue-red color scale.

To sum up all of these results, Figure 16 shows the improvements on each state variable (WSE, FWE and Q) when different SWOT-like observations are assimilated. Performance obtained by assimilating absolute values or anomalies are also compared in this figure. It is important to highlight that the major improvements occur when the same state variable is assimilated (e.g. improvements in Q when SWOT-like Q is assimilated) for both, absolute and anomalies assimilation set up. Besides, the assimilation of absolute values of FWE has the large amplitude on ΔRRMSE between variables. It is even degrading Q, as explained in section 6.3. The multi-variable assimilation is noticed to be the best set up when absolute values are assimilated. The assimilation of anomalies shows less dispersion on ΔRRMSE between all variables. Finally, anomaly of WSE (WSE') seems to be the optimal set up for SWOT assimilation purposes.

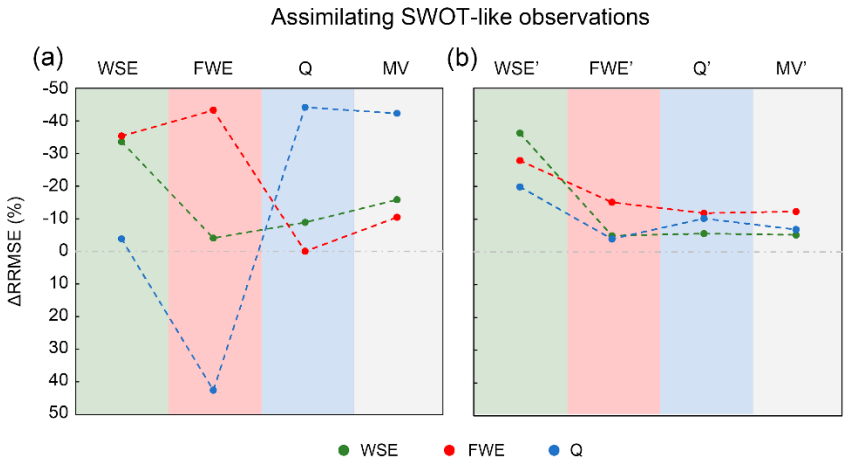

Figure 16. Median values (dots) of improvements on each state variables when different SWOT-like observations are assimilated (color translucid bars).

7. Conclusions and perspectives

This research aimed to implement and assess DA of SWOT-like observations within a large-scale hydrological model that emulates the uncertainties of GHMs. In order to do this, the large-scale SWOT pixel cloud simulator and a basin with a complex drainage network were chosen.

Perturbation strategies were performed so as to achieve the values of uncertainties of the GHMs. The main representative source of errors from forcings and parameters of the model were therefore considered. Analyses are therefore valid for other basins, as we emulate errors of GHMs. Results shows that the main sources of global model discharge errors are precipitation and water budget parameters uncertainty. These can achieve around 40% and 30% of RRMSE respectively, which is larger than the other sources of errors and could represent ~50-70% of all of the total uncertainty. Besides, the main

source of global model WSE error are the hydraulic parameters as bathymetry (depth, width and manning coefficient), which represent ~50% of the total uncertainty.

Once the performance of SWOT DA relies on sources of hydrological model errors, the sensitivity analysis of the improvements on the state variables of the model regarding individual error scenarios were assessed. It was observed that the hydraulic parameters and the floodplain topography were the worst scenarios for the performance in Q when WSE and FWE were assimilated; which depict the strong influence of these parameters in Q simulation. Besides, the only aggravation on WSE was figured out when the FWE was assimilated in the scenario of errors of floodplain topography that also relates the large relation among WSE, FWE and floodplain due to the hypsometric curve used in our hydraulic simulations.

Different approaches for ingest SWOT-like observations showed a suitable way in which to use these data in the future for GHMs. For instance, when the full-sources error model is assessed, which means an emulated GHM, improvements in some state variables of the model were not achieved by the assimilation of individual SWOT-like observations; as in the case when the assimilation of FWE degrades discharge. In addition, the improvements in discharge by assimilating SWOT-like Q on a global scale were larger than other assessments (assimilation WSE or FWE). Hence, assuming that SWOT products of Q are as accurate as the most optimistic values of uncertainty so far shown in the literature, they may be able to improve simulations by using global and continental scale hydrological models by approximately ~40%. For the assimilation of SWOT-like WSE, the importance of a better estimation of hydraulic parameters before the estimation of discharge (e.g. for hydrodynamic models) was noted.

The improvements of all state variables were only reached by the use of the multi-variable DA scheme, which can be explained due to the assimilation of different SWOT-like at the same time which can constrain their individual uncertainties. This is even the case when the uncorrelated observations were assumed as a simplification in this study.

The improvements by the use of anomalies of SWOT-like observations were assessed. Experiments assimilating WSE' showed the best improvements for all state variables. Its application may be restricted however to hydrological models which incorporate a hydrodynamic routing module. Besides, the assimilation of FWE' and Q' improved all state variables, although these were not greater than when absolute values were assimilated for the cases of the correspondent state variable (e.g. improvements on Q by assimilating SWOT-like Q).

A smart combination of assimilation of SWOT-like observations should be considered regarding the uncertainties of GHMs. Hence, the correction of the model parameters that impact most on uncertainty (e.g. hydrologic, hydraulic) should also be taken into consideration. Given the large amount of information that SWOT will provide, other less computationally demanding assimilation schemes (e.g. ensemble square-root Kalman Filter) should be assessed. As well as more complex methods for estimating the covariance matrix of the background error.

Finally, other approaches should be implemented in the future when real SWOT data are available such as further exploration of the multi-variable DA technique through the use of less simplified assumptions, for example, to assume a certain correlation between different observations. Even under large uncertainties by GHMs however, SWOT data show that it could have a great impact on improvements in hydrological and

hydrodynamic simulations on a global and continental scale; this implies a promising utility for the SWOT scientific community.

Declaration of interest

The authors declare no conflict of interest.

The funders had no role in the design of the study; in the collection, analyses, or interpretation of data; in the writing of the manuscript, or in the decision to publish the results.

Acknowledgments

The first author is grateful for a grant from the Brazilian agency CAPES.

LEGOS (Laboratoire d'Etudes en Géophysique et Océanographie Spatiales) and GET (Laboratoire Géosciences Environnement Toulouse) are also thanked for their logistic support during the first author doctoral internship in France.

We would also like to thank Damien Desroches from CNES who provided the SWOT simulator software called "Large Scale Level 2 HR Pixel Cloud Simulator".

This research was in the context of the SWOT-MOD science team project from SWOT satellite mission.

This work was partially supported by CNES.

We would also like to thank two anonymous reviewers for their comments, which have helped significantly in the improvement of this manuscript.

References

Albernaz, A.L.K.M., Venticinque, E.., 2003. Reserva de Desenvolvimento Sustentável Piagaçu-Purus: Características e Limites Geográficos In Piagaçu-Purus, in: Bases Científicas Para Criação de Uma Reserva de Desenvolvimento Sustentável. pp. 3–12.

Alsdorf, D., Lettenmaier, D., Vorosmarty, C., 2003. The need for global, satellite- based observations of terrestrial surface waters. Eos (Washington. DC). 84. https://doi.org/10.1029/2003EO290001

Alsdorf, D.E., Rodríguez, E., Lettenmaier, D.P., 2007. Measuring surface water from space. Rev. Geophys. 45, RG2002. https://doi.org/10.1029/2006RG000197

Andreadis, K.M., Clark, E.A., Lettenmaier, D.P., Alsdorf, D.E., 2007. Prospects for river discharge and depth estimation through assimilation of swath-altimetry into a raster-based hydrodynamics model. Geophys. Res. Lett. 34, 1–5. https://doi.org/10.1029/2007GL029721

Andreadis, K.M., Das, N., Stampoulis, D., Ines, A., Fisher, J.B., Granger, S., Kawata, J., Han, E., Behrangi, A., 2017. The regional hydrologic extremes assessment system: A software framework for hydrologic modeling and data assimilation. PLoS One 12, 1–22. https://doi.org/10.1371/journal.pone.0176506

Andreadis, K.M., Schumann, G.J.P., 2014. Estimating the impact of satellite observations on the predictability of large-scale hydraulic models. Adv. Water Resour. 73, 44–54. https://doi.org/10.1016/j.advwatres.2014.06.006

Andreadis, K.M., Schumann, G.J.P., Pavelsky, T., 2013. A simple global river bankfull width and depth database. Water Resour. Res. 49, 7164–7168. https://doi.org/10.1002/wrcr.20440

Anees, M.T., Abdullah, K., Nordin, M.N.M., Rahman, N.N.N.A., Syakir, M.I., Kadir, M.O.A., 2017. One- and Two-Dimensional Hydrological Modelling and Their Uncertainties, in: Flood Risk Management. InTech, pp. 1–30. https://doi.org/10.5772/intechopen.68924

Baguis, P., Roulin, E., 2017. Soil moisture data assimilation in a hydrological model: A case study in Belgium using large-scale satellite data. Remote Sens. 9, 1–26. https://doi.org/10.3390/rs9080820

Balsamo, G., Viterbo, P., Beijaars, A., van den Hurk, B., Hirschi, M., Betts, A.K., Scipal, K., 2009. A revised hydrology for the ECMWF model: Verification from field site to terrestrial water storage and impact in the integrated forecast system. J. Hydrometeorol. 10, 623–643. https://doi.org/10.1175/2008JHM1068.1

Baratelli, F., Flipo, N., Rivière, A., Biancamaria, S., 2018. Retrieving river baseflow from SWOT spaceborne mission. Remote Sens. Environ. 218, 44–54. https://doi.org/10.1016/j.rse.2018.09.013

Bates, P.D., Horritt, M.S., Fewtrell, T.J., 2010. A simple inertial formulation of the shallow water equations for efficient two-dimensional flood inundation modelling. J. Hydrol. 387, 33–45. https://doi.org/10.1016/j.jhydrol.2010.03.027

Beck, H.E., van Dijk, A.I.J.M., Levizzani, V., Schellekens, J., Miralles, D.G., Martens, B., de Roo, A., 2016. MSWEP: 3-hourly 0.25° global gridded precipitation (1979–2015) by merging gauge, satellite, and reanalysis data. Hydrol. Earth Syst. Sci. Discuss. 1–38. https://doi.org/10.5194/hess-2016-236

Biancamaria, S., Durand, M., Andreadis, K.M., Bates, P.D., Boone, A., Mognard, N.M., Rodríguez, E., Alsdorf, D.E., Lettenmaier, D.P., Clark, E.A., 2011. Assimilation of virtual wide swath altimetry to improve Arctic river modeling. Remote Sens. Environ. 115, 373–381. https://doi.org/10.1016/j.rse.2010.09.008

Biancamaria, S., Frappart, F., Leleu, A.-S., Marieu, V., Blumstein, D., Desjonquères, J.-D., Boy, F., Sottolichio, A., Valle-Levinson, A., 2017. Satellite radar altimetry water elevations performance over a 200m wide river: Evaluation over the Garonne River. Adv. Sp. Res. 59, 128–146. https://doi.org/https://doi.org/10.1016/j.asr.2016.10.008

Biancamaria, S., Lettenmaier, D.P., Pavelsky, T.M., 2016. The SWOT Mission and Its Capabilities for Land Hydrology. Surv. Geophys. 37, 307–337. https://doi.org/10.1007/s10712-015-9346-y

Bjerklie, D.M., Dingman, S.L., Bolster, C.H., 2005. Comparison of constitutive flow resistance equations based on the Manning and Chezy equations applied to natural rivers 41, 1–7. https://doi.org/10.1029/2004WR003776

Bonnema, M., Hossain, F., 2019. Assessing the Potential of the Surface Water and Ocean Topography Mission for Reservoir Monitoring in the Mekong River Basin. Water Resour. Res. 55, 444–461. https://doi.org/10.1029/2018WR023743

Bonnema, M.G., Sikder, S., Hossain, F., Durand, M., Gleason, C.J., Bjerklie, D.M., 2016. Benchmarking wide swath altimetry-based river discharge estimation algorithms for the Ganges river system. Water Resour. Res. https://doi.org/10.1002/2015WR017296

Brêda, J.P.L.F., Paiva, R.C.D., Bravo, J.M., Passaia, O.A., Moreira, D.M., 2019. Assimilation of Satellite Altimetry Data for Effective River Bathymetry. Water Resour. Res. 55, 7441–7463. https://doi.org/10.1029/2018WR024010

Burgers, G., Van Leeuwen, P.J., Evensen, G., 1998. Analysis scheme in the ensemble Kalman filter. Mon. Weather Rev. 126, 1719–1724. https://doi.org/10.1175/1520-0493(1998)126<1719:ASITEK>2.0.CO;2

Chen, H., Yang, D., Hong, Y., Gourley, J.J., Zhang, Y., 2013. Hydrological data assimilation with the Ensemble Square-Root-Filter: Use of streamflow observations to update model states for real-time flash flood forecasting. Adv. Water Resour. 59, 209–220. https://doi.org/https://doi.org/10.1016/j.advwatres.2013.06.010

Chevalier, L., Desroches, D., Laignel, B., Fjørtoft, R., Turki, I., Allain, D., Lyard, F., Blumstein, D., Salameh, E., 2019. High-Resolution SWOT Simulations of the Macrotidal Seine Estuary in Different Hydrodynamic Conditions. IEEE Geosci. Remote Sens. Lett. 16, 5–9. https://doi.org/10.1109/LGRS.2018.2862470

Clark, M.P., Rupp, D.E., Woods, R.A., Zheng, X., Ibbitt, R.P., Slater, A.G., Schmidt, J., Uddstrom, M.J., 2008. Hydrological data assimilation with the ensemble Kalman filter: Use of streamflow observations to update states in a distributed hydrological model. Adv. Water Resour. 31, 1309–1324. https://doi.org/10.1016/j.advwatres.2008.06.005

Collischonn, W., Allasia, D., da Silva, B.C., Tucci, C.E.M., 2007. The MGB-IPH model for large-scale rainfall-runoff modelling. Hydrol. Sci. J. 52, 878–895. https://doi.org/10.1623/hysj.52.5.878

Crow, W.T., Ryu, D., 2008. A new data assimilation approach for improving hydrologic prediction using remotely-sensed soil moisture retrievals. Hydrol. Earth Syst. Sci. Discuss. 5, 2005–2044. https://doi.org/10.5194/hessd-5-2005-2008

David, C.H., Maidment, D.R., Niu, G.Y., Yang, Z.L., Habets, F., Eijkhout, V., 2011. River network routing on the NHDPlus dataset. J. Hydrometeorol. 12, 913–934. https://doi.org/10.1175/2011JHM1345.1

de Paiva, R.C.D., Buarque, D.C., Collischonn, W., Bonnet, M.-P., Frappart, F., Calmant, S., Bulhões Mendes, C.A., 2013. Large-scale hydrologic and hydrodynamic modeling of the Amazon River basin. Water Resour. Res. 49, 1226–1243. https://doi.org/10.1002/wrcr.20067

Desai, S., 2018. Surface Water and Ocean Topography Mission Project Science Requirements Document. Jet Propuls. Lab.

Desroches, D., Pottier, C., Blumstein, D., Biancamaria, S., Poughon, V., Fjortoft, R., 2018. Large Scale Pixel Cloud Simulator and Hydrology Toolbox, in: SWOT Science Team Meeting, Montreal Canada 23 June. Montreal Canada 23 June.

Döll, P., Berkhoff, K., Bormann, H., Fohrer, N., Gerten, D., Hagemann, S., Krol, M., 2008. Advances and visions in large-scale hydrological modelling: Findings from the 11th Workshop on Large-Scale Hydrological Modelling. Adv. Geosci. 18, 51–61. https://doi.org/10.5194/adgeo-18-51-2008

Döll, P., Fiedler, K., Zhang, J., 2009. Global-scale analysis of river flow alterations due to water withdrawals and reservoirs. Hydrol. Earth Syst. Sci. 13, 2413–2432. https://doi.org/10.5194/hess-13-2413-2009

Domeneghetti, A., Schumann, G.J.-P., Frasson, R.P.M., Wei, R., Pavelsky, T.M., Castellarin, A., Brath, A., Durand, M.T., 2018. Characterizing water surface elevation under different flow conditions for the upcoming SWOT mission. J. Hydrol. 561, 848–861. https://doi.org/https://doi.org/10.1016/j.jhydrol.2018.04.046

Durand, M., Andreadis, K.M., Alsdorf, D.E., Lettenmaier, D.P., Moller, D., Wilson, M., 2008. Estimation of bathymetric depth and slope from data assimilation of swath altimetry into a hydrodynamic model. Geophys. Res. Lett. 35, 1–5. https://doi.org/10.1029/2008GL034150

Durand, M., Fu, L.L., Lettenmaier, D.P., Alsdorf, D.E., Rodriguez, E., Esteban-Fernandez, D., 2010. The surface water and ocean topography mission: Observing terrestrial surface water and oceanic submesoscale eddies. Proc. IEEE 98, 766–779. https://doi.org/10.1109/JPROC.2010.2043031

Durand, M., Gleason, C.J., Garambois, P.A., Bjerklie, D., Smith, L.C., Roux, H., Rodriguez, E., Bates, P.D., Pavelsky, T.M., Monnier, J., Chen, X., Di Baldassarre, G., Fiset, J.-M., Flipo, N., Frasson, R.P. d. M., Fulton, J., Goutal, N., Hossain, F., Humphries, E., Minear, J.T., Mukolwe, M.M., Neal, J.C., Ricci, S., Sanders, B.F., Schumann, G., Schubert, J.E., Vilmin, L., 2016. An intercomparison of remote sensing river discharge estimation algorithms from measurements of river height, width, and slope. Water Resour. Res. 52, 4527–4549. https://doi.org/10.1002/2015WR018434

Emery, C.M., Paris, A., Biancamaria, S., Boone, A., Calmant, S., Garambois, P.A., Da Silva, J.S., 2018. Large-scale hydrological model river storage and discharge correction using a

satellite altimetry-based discharge product. Hydrol. Earth Syst. Sci. 22, 2135–2162. https://doi.org/10.5194/hess-22-2135-2018

Engman, E.T., 1995. Recent advances in remote sensing in hydrology. Rev. Geophys. 33, 967–975. https://doi.org/10.1029/95RG00403

Evensen, G., 2004. Sampling strategies and square root analysis schemes for the EnKF. Ocean Dyn. 54, 539–560. https://doi.org/10.1007/s10236-004-0099-2

Evensen, G., 2003. The Ensemble Kalman Filter: Theoretical formulation and practical implementation. Ocean Dyn. 53, 343–367. https://doi.org/10.1007/s10236-003-0036-9

Evensen, G., 1994. Sequential data assimilation with a nonlinear quasi-geostrophic model using Monte Carlo methods to forecast error statistics. J. Geophys. Res. 99. https://doi.org/10.1029/94jc00572

Farr, T.G., Rosen, P.A., Caro, E., Crippen, R., Duren, R., Hensley, S., Kobrick, M., Paller, M., Rodriguez, E., Roth, L., Seal, D., Shaffer, S., Shimada, J., Umland, J., Werner, M., Oskin, M., Burbank, D., Alsdorf, D., 2007. The Shuttle Radar Topography Mission 1–33. https://doi.org/10.1029/2005RG000183.1.INTRODUCTION

Fernandez, D.E., Pollard, B., Steunou, N., 2017. SWOT Project.

Fisher, C.K., Pan, M., Wood, E.F., 2018. Spatiotemporal Assimilation/Interpolation of Discharge Records through Inverse Streamflow Routing. Hydrol. Earth Syst. Sci. Discuss. 1–23. https://doi.org/10.5194/hess-2018-109

Fleischmann, A., Paiva, R., Collischonn, W., 2019. Can regional to continental river hydrodynamic models be locally relevant? A cross-scale comparison. J. Hydrol. X 3, 100027. https://doi.org/10.1016/j.hydroa.2019.100027

Frasson, R.P. de M., Wei, R., Durand, M., Minear, J.T., Domeneghetti, A., Schumann, G., Williams, B.A., Rodriguez, E., Picamilh, C., Lion, C., Pavelsky, T., Garambois, P.A., 2017. Automated River Reach Definition Strategies: Applications for the Surface Water and Ocean Topography Mission. Water Resour. Res. 53, 8164–8186. https://doi.org/10.1002/2017WR020887

Gao, H., Tang, Q., Shi, X., Zhu, C., Bohn, T., Su, F., Sheffield, J., Pan, M., Lettenmaier, D., Wood, E.F., 2010. Water Budget Record from Variable Infiltration Capacity (VIC) Model, in: Algorithm Theoretical Basis Document for Terrestrial Water Cycle Data Records. pp. 120–173.

Garambois, P.-A., Larnier, K., Monnier, J., Finaud-Guyot, P., Verley, J., Montazem, A.-S., Calmant, S., 2019. Variational inference of effective channel and ungauged anabranching river discharge from multi-satellite water heights of different spatial sparsity. J. Hydrol. 124409. https://doi.org/https://doi.org/10.1016/j.jhydrol.2019.124409

Getirana, A., Peters-Lidard, C., Rodell, M., Bates, P.D., 2017. Trade-off between cost and accuracy in large-scale surface water dynamic modeling. Water Resour. Res. 53, 4942–4955. https://doi.org/10.1002/2017WR020519

Gleason, C.J., Wada, Y., Wang, J., 2018. A Hybrid of Optical Remote Sensing and Hydrological Modeling Improves Water Balance Estimation. J. Adv. Model. Earth Syst. 10, 2–17. https://doi.org/10.1002/2017MS000986

Goulding, M., Barthem, R., Ferreira, E., 2003. The Smithsonian Atlas of the Amazon. Smithsonian Institution Press.

Grippa, M., Rouzies, C., Biancamaria, S., Blumstein, D., Cretaux, J., Gal, L., Robert, E., Gosset, M., Kergoat, L., 2019. Potential of SWOT for Monitoring Water Volumes in Sahelian Ponds and Lakes. IEEE J. Sel. Top. Appl. Earth Obs. Remote Sens. 12, 2541–2549. https://doi.org/10.1109/JSTARS.2019.2901434

Gupta, H.V., Sorooshian, S., Yapo, P.O., 1998. Toward improved calibration of hydrologic models: Multiple and noncommensurable measures of information. Water Resour. Res. 34, 751–763.

Herschy, R.W., 2002. The uncertainty in a current meter measurement. Flow Meas. Instrum. 13, 281–284. https://doi.org/https://doi.org/10.1016/S0955-5986(02)00047-X

Houtekamer, P.L., Mitchell, H.L., 2001. A Sequential Ensemble Kalman Filter for Atmospheric Data Assimilation. Mon. Weather Rev. 129, 123–137. https://doi.org/10.1175/1520-0493(2001)129<0123:ASEKFF>2.0.CO;2

Kauffeldt, A., Wetterhall, F., Pappenberger, F., Salamon, P., Thielen, J., 2016. Technical review of large-scale hydrological models for implementation in operational flood forecasting schemes on continental level. Environ. Model. Softw. 75, 68–76. https://doi.org/10.1016/j.envsoft.2015.09.009

Khaki, M., Forootan, E., Kuhn, M., Awange, J., Papa, F., Shum, C.K., 2018. A study of Bangladesh's sub-surface water storages using satellite products and data assimilation scheme. Sci. Total Environ. 625, 963–977. https://doi.org/10.1016/j.scitotenv.2017.12.289

Khaki, M., Hoteit, I., Kuhn, M., Forootan, E., Awange, J., 2019. Assessing data assimilation frameworks for using multi-mission satellite products in a hydrological context. Sci. Total Environ. 647, 1031–1043. https://doi.org/10.1016/j.scitotenv.2018.08.032

Lai, X., Liang, Q., Yesou, H., Daillet, S., 2014. Variational assimilation of remotely sensed flood extents using a 2-D flood model. Hydrol. Earth Syst. Sci. 18, 4325–4339. https://doi.org/10.5194/hess-18-4325-2014

Langhorst, T., Pavelsky, T.M., Frasson, R.P. de M., Wei, R., Domeneghetti, A., Altenau, E.H., Durand, M.T., Minear, J.T., Wegmann, K.W., Fuller, M.R., 2019. Anticipated improvements to river surface elevation profiles from the surface water and ocean topography mission. Front. Earth Sci. 7, 1–13. https://doi.org/10.3389/feart.2019.00102

Latrubesse, E.M., 2008. Patterns of anabranching channels: The ultimate end-member adjustment of mega rivers. Geomorphology 101, 130–145. https://doi.org/10.1016/j.geomorph.2008.05.035

Legresy, B., Papa, F., Remy, F., Vinay, G., van den Bosch, M., Zanife, O.-Z., 2005. ENVISAT radar altimeter measurements over continental surfaces and ice caps using the ICE-2 retracking algorithm. Remote Sens. Environ. 95, 150–163. https://doi.org/https://doi.org/10.1016/j.rse.2004.11.018

Liu, Y., Weerts, A.H., Clark, M., Hendricks Franssen, H.J., Kumar, S., Moradkhani, H., Seo, D.J., Schwanenberg, D., Smith, P., Van Dijk, A.I.J.M., Van Velzen, N., He, M., Lee, H., Noh, S.J., Rakovec, O., Restrepo, P., 2012. Advancing data assimilation in operational hydrologic forecasting: Progresses, challenges, and emerging opportunities. Hydrol. Earth Syst. Sci. 16, 3863–3887. https://doi.org/10.5194/hess-16-3863-2012

López, P.L., Sutanudjaja, E.H., Schellekens, J., Sterk, G., Bierkens, M.F.P., 2017. Calibration of a large-scale hydrological model using satellite-based soil moisture and evapotranspiration products. Hydrol. Earth Syst. Sci. 21, 3125–3144. https://doi.org/10.5194/hess-21-3125-2017

Loukas, A., Vasiliades, L., 2014. Streamflow simulation methods for ungauged and poorly gauged watersheds. Nat. Hazards Earth Syst. Sci. 14, 1641–1661. https://doi.org/10.5194/nhess-14-1641-2014

Madsen, H., 2000. Automatic calibration of a conceptual rainfall–runoff model using multiple objectives. J. Hydrol. 235, 276–288. https://doi.org/https://doi.org/10.1016/S0022-1694(00)00279-1

Marengo, J.A., Espinoza, J.C., 2016. Extreme seasonal droughts and floods in Amazonia: Causes, trends and impacts. Int. J. Climatol. 36, 1033–1050. https://doi.org/10.1002/joc.4420

Massari, C., Brocca, L., Tarpanelli, A., Moramarco, T., 2015. Data assimilation of satellite soil moisture into rainfall-runoffmodelling: A complex recipe?, Remote Sensing. https://doi.org/10.3390/rs70911403

McClain, M.E., Naiman, R.J., 2008. Andean Influences on the Biogeochemistry and Ecology of the Amazon River. Bioscience 58, 325–338. https://doi.org/10.1641/b580408

Meade, R.H., Rayol, J.M., Da Conceicão, S.C., Natividade, J.R.G., 1991. Backwater effects in the Amazon River basin of Brazil. Environ. Geol. Water Sci. 18, 105–114. https://doi.org/10.1007/BF01704664

Michailovsky, C.I., Milzow, C., Bauer-Gottwein, P., 2013. Assimilation of radar altimetry to a routing model of the Brahmaputra River. Water Resour. Res. 49, 4807–4816. https://doi.org/10.1002/wrcr.20345

Moody, J.A., Troutman, B.M., 2002. Characterization of the spatial variability of channel morphology. Earth Surf. Process. Landforms 27, 1251–1266. https://doi.org/10.1002/esp.403

Munier, S., Polebistki, A., Brown, C., Belaud, G., Lettenmaier, D.P., 2015. SWOT data assimilation for operational reservoir management on the upper Niger River Basin. Water Resour. Res. 51, 554–575. https://doi.org/10.1002/2014WR016157

Neal, J.C., Atkinson, P.M., Hutton, C.W., 2007. Flood inundation model updating using an ensemble Kalman filter and spatially distributed measurements. J. Hydrol. 336, 401–415. https://doi.org/https://doi.org/10.1016/j.jhydrol.2007.01.012

Neppel, L., Renard, B., Lang, M., Ayral, P.A., Coeur, D., Gaume, E., Jacob, N., Payrastre, O., Pobanz, K., Vinet, F., 2010. Flood frequency analysis using historical data: Accounting for random and systematic errors. Hydrol. Sci. J. 55, 192–208. https://doi.org/10.1080/02626660903546092

New, M., Lister, D., Hulme, M., Makin, I., 2002. A high-resolution data set of surface climate over global land areas. Clim. Res. 21, 1–25. https://doi.org/10.3354/cr021001

Nijssen, B., Lettenmaier, D.P., 2004. Effect of precipitation sampling error on simulated hydrological fluxes and states: Anticipating the Global Precipitation Measurement satellites. J. Geophys. Res. D Atmos. 109, 1–15. https://doi.org/10.1029/2003jd003497

Nijzink, R.C., Almeida, S., Pechlivanidis, I.G., Capell, R., Gustafssons, D., Arheimer, B., Parajka, J., Freer, J., Han, D., Wagener, T., Nooijen, R.R.P., Savenije, H.H.G., Hrachowitz, M., 2018. Constraining Conceptual Hydrological Models With Multiple Information Sources. Water Resour. Res. 54, 8332–8362. https://doi.org/10.1029/2017WR021895

O'Loughlin, F.E., Paiva, R.C.D., Durand, M., Alsdorf, D.E., Bates, P.D., 2016. A multi-sensor

approach towards a global vegetation corrected SRTM DEM product. Remote Sens. Environ. 182, 49–59. https://doi.org/10.1016/j.rse.2016.04.018

Oubanas, H., Gejadze, I., Malaterre, P.O., Durand, M., Wei, R., Frasson, R.P.M., Domeneghetti, A., 2018a. Discharge Estimation in Ungauged Basins Through Variational Data Assimilation: The Potential of the SWOT Mission. Water Resour. Res. 54, 2405–2423. https://doi.org/10.1002/2017WR021735

Oubanas, H., Gejadze, I., Malaterre, P.O., Mercier, F., 2018b. River discharge estimation from synthetic SWOT-type observations using variational data assimilation and the full Saint-Venant hydraulic model. J. Hydrol. 559, 638–647. https://doi.org/10.1016/j.jhydrol.2018.02.004

Paiva, R.C.D., Collischonn, W., Bonnet, M.-P., de Gonçalves, L.G.G., Calmant, S., Getirana, A., Santos da Silva, J., 2013. Assimilating in situ and radar altimetry data into a large-scale hydrologic-hydrodynamic model for streamflow forecast in the Amazon. Hydrol. Earth Syst. Sci. 17, 2929–2946. https://doi.org/10.5194/hess-17-2929-2013

Paiva, R.C.D., Collischonn, W., Tucci, C.E.M., 2011. Large scale hydrologic and hydrodynamic modeling using limited data and a GIS based approach. J. Hydrol. 406, 170–181. https://doi.org/10.1016/j.jhydrol.2011.06.007

Paiva, R.C.D., Durand, M.T., Hossain, F., 2015. Spatiotemporal interpolation of discharge across a river network by using synthetic SWOT satellite data. Water Resour. Res. 51, 430–449. https://doi.org/10.1002/2014WR015618

Papa, F., Legrésy, B., Rémy, F., 2003. Use of the Topex–Poseidon dual-frequency radar altimeter over land surfaces. Remote Sens. Environ. 87, 136–147. https://doi.org/https://doi.org/10.1016/S0034-4257(03)00136-6

Paris, A., Dias de Paiva, R., Santos da Silva, J., Medeiros Moreira, D., Calmant, S., Garambois, P.-A., Collischonn, W., Bonnet, M.-P., Seyler, F., 2016. Stage-discharge rating curves based on satellite altimetry and modeled discharge in the Amazon basin. Water Resour. Res. 52, 3787–3814. https://doi.org/10.1002/2014WR016618

Pedinotti, V., Boone, A., Ricci, S., Biancamaria, S., Mognard, N., 2014. Assimilation of satellite data to optimize large-scale hydrological model parameters: A case study for the SWOT mission. Hydrol. Earth Syst. Sci. 18, 4485–4507. https://doi.org/10.5194/hess-18-4485-2014

Pelletier, P.M., 1988. Uncertainties in the single determination of river discharge: a literature review. Can. J. Civ. Eng. 15, 834–850. https://doi.org/10.1139/l88-109

Peral, E., Rodríguez, E., Moller, D., McAdams, M., Johnson, M., Andreadis, K., Arumugan, D., Williams, B., 2016. SWOT simulator quick user guide, version 2.2, Document number D-79123.

Pontes, P.R.M., Fan, F.M., Fleischmann, A.S., de Paiva, R.C.D., Buarque, D.C., Siqueira, V.A., Jardim, P.F., Sorribas, M.V., Collischonn, W., 2017. MGB-IPH model for hydrological and hydraulic simulation of large floodplain river systems coupled with open source GIS. Environ. Model. Softw. 94, 1–20. https://doi.org/10.1016/j.envsoft.2017.03.029

Reichle, R.H., 2008. Data assimilation methods in the Earth sciences. Adv. Water Resour. 31, 1411–1418. https://doi.org/10.1016/j.advwatres.2008.01.001

Revel, M., Ikeshima, D., Yamazaki, D., Kanae, S., 2019. A physically based empirical localization method for assimilating synthetic SWOT observations of a continental-scale river: A case study in the Congo basin. Water (Switzerland) 11.

https://doi.org/10.3390/w11040829

Revilla-Romero, B., Wanders, N., Burek, P., Salamon, P., de Roo, A., 2016. Integrating remotely sensed surface water extent into continental scale hydrology. J. Hydrol. 543, 659–670. https://doi.org/10.1016/j.jhydrol.2016.10.041

Schmidt, A.R., 2002. Analysis of Stage-Discharge Relations for Open -Channel Flows and Their Associated Uncertainties. University of Illinois at Urbana-Champaign.

Sheil, D., 2018. Forests, atmospheric water and an uncertain future: the new biology of the global water cycle. For. Ecosyst. 5, 19. https://doi.org/10.1186/s40663-018-0138-y

Siqueira, V.A., Paiva, R.C.D., Fleischmann, A.S., Fan, F.M., Ruhoff, A.L., Pontes, P.R.M., Paris, A., Calmant, S., Collischonn, W., 2018. Toward continental hydrologic-hydrodynamic modeling in South America. Hydrol. Earth Syst. Sci. 22, 4815–4842. https://doi.org/10.5194/hess-22-4815-2018

Sivapalan, M., 2003. Prediction in ungauged basins: a grand challenge for theoretical hydrology. Hydrol. Process. 17, 3163–3170. https://doi.org/10.1002/hyp.5155

Solander, K.C., Reager, J.T., Famiglietti, J.S., 2016. How well will the Surface Water and Ocean Topography (SWOT) mission observe global reservoirs? Water Resour. Res. 52, 2123–2140. https://doi.org/10.1002/2015WR017952

Sood, A., Smakhtin, V., 2015. Global hydrological models: a review. Hydrol. Sci. J. 60, 549–565. https://doi.org/10.1080/02626667.2014.950580

Sun, L., Seidou, O., Nistor, I., Liu, K., 2016. Review of the Kalman-type hydrological data assimilation. Hydrol. Sci. J. 61, 2348–2366. https://doi.org/10.1080/02626667.2015.1127376

Sun, Q., Miao, C., Duan, Q., Ashouri, H., Sorooshian, S., Hsu, K., 2018. A Review of Global Precipitation Data Sets: Data Sources, Estimation, and Intercomparisons. Rev. Geophys. 56, 79–107. https://doi.org/10.1002/2017RG000574

Tang, Q., Gao, H., Lu, H., Lettenmaier, D.P., 2009. Remote sensing: Hydrology. Prog. Phys. Geogr. 33, 490–509. https://doi.org/10.1177/0309133309346650

Thielen-Del Pozo, J., Pappenberger, F., Salamon, P., Bogner, K., Burek, P., de Roo, A., 2010. The state of the art of flood forecasting - Hydrological Ensemble Prediction Systems, in: 10th EMS Annual Meeting. pp. EMS2010-145.

Todini, E., 1996. The ARNO rainfall—runoff model. J. Hydrol. 175, 339–382. https://doi.org/https://doi.org/10.1016/S0022-1694(96)80016-3

Trigg, M.A., Wilson, M.D., Bates, P.D., Horritt, M.S., Alsdorf, D.E., Forsberg, B.R., Vega, M.C., 2009. Amazon flood wave hydraulics. J. Hydrol. 374, 92–105. https://doi.org/10.1016/j.jhydrol.2009.06.004

Tuozzolo, S., Lind, G., Overstreet, B., Mangano, J., Fonstad, M., Hagemann, M., Frasson, R.P.M., Larnier, K., Garambois, P.A., Monnier, J., Durand, M., 2019. Estimating River Discharge With Swath Altimetry: A Proof of Concept Using AirSWOT Observations. Geophys. Res. Lett. 46, 1459–1466. https://doi.org/10.1029/2018GL080771

Van Der Knijff, J.M., Younis, J., De Roo, A.P.J., 2010. LISFLOOD: a GIS-based distributed model for river basin scale water balance and flood simulation. Int. J. Geogr. Inf. Sci. 24, 189–212. https://doi.org/10.1080/13658810802549154

van Dijk, A.I.J.M., Renzullo, L.J., 2011. Water resource monitoring systems and the role of satellite observations. Hydrol. Earth Syst. Sci. 15, 39–55. https://doi.org/10.5194/hess-15-39-2011

Wanders, N., Bierkens, M.F.P., de Jong, S.M., de Roo, A., Karssenberg, D., 2014. The benefits of using remotely sensed soil moisture in parameter identification of large-scale hydrological models. Water Resour. Res. 50, 6874–6891. https://doi.org/10.1002/2013WR014639

Wongchuig, S.C., de Paiva, R.C.D., Siqueira, V., Collischonn, W., 2019. Hydrological reanalysis across the 20th century: A case study of the Amazon Basin. J. Hydrol. 570, 755–773. https://doi.org/10.1016/j.jhydrol.2019.01.025

Wood, E.F., Roundy, J.K., Troy, T.J., van Beek, L.P.H., Bierkens, M.F.P., Blyth, E., de Roo, A., Döll, P., Ek, M., Famiglietti, J., Gochis, D., van de Giesen, N., Houser, P., Jaffé, P.R., Kollet, S., Lehner, B., Lettenmaier, D.P., Peters-Lidard, C., Sivapalan, M., Sheffield, J., Wade, A., Whitehead, P., 2011. Hyperresolution global land surface modeling: Meeting a grand challenge for monitoring Earth's terrestrial water. Water Resour. Res. 47, 1–10. https://doi.org/10.1029/2010WR010090

Xue, M., Jung, Y., Zhang, G., 2007. Error modeling of simulated reflectivity observations for ensemble Kalman filter assimilation of convective storms. Geophys. Res. Lett. 34, 1–5. https://doi.org/10.1029/2007GL029945

Yamazaki, D., de Almeida, G.A.M., Bates, P.D., 2013. Improving computational efficiency in global river models by implementing the local inertial flow equation and a vector-based river network map. Water Resour. Res. 49, 7221–7235. https://doi.org/10.1002/wrcr.20552

Yamazaki, D., Ikeshima, D., Tawatari, R., Yamaguchi, T., O'Loughlin, F., Neal, J.C., Sampson, C.C., Kanae, S., Bates, P.D., 2017. A high-accuracy map of global terrain elevations. Geophys. Res. Lett. 44, 5844–5853. https://doi.org/10.1002/2017GL072874

Yamazaki, D., Kanae, S., Kim, H., Oki, T., 2011. A physically based description of floodplain inundation dynamics in a global river routing model. Water Resour. Res. 47, 1–21. https://doi.org/10.1029/2010WR009726

Yang, Y., Lin, P., Fisher, C.K., Turmon, M., Hobbs, J., Emery, C.M., Reager, J.T., David, C.H., Lu, H., Yang, K., Hong, Y., Wood, E.F., Pan, M., 2019. Enhancing SWOT discharge assimilation through spatiotemporal correlations. Remote Sens. Environ. 234, 111450. https://doi.org/10.1016/j.rse.2019.111450

Yoon, Y., Durand, M., Merry, C.J., Clark, E.A., Andreadis, K.M., Alsdorf, D.E., 2012. Estimating river bathymetry from data assimilation of synthetic SWOT measurements. J. Hydrol. 464–465, 363–375. https://doi.org/10.1016/j.jhydrol.2012.07.028

Yoon, Y., Durand, M., Merry, C.J., Rodr\iguez, E., 2013. Improving temporal coverage of the SWOT mission using spatiotemporal kriging, IEEE J. Sel 6, 1719–1729. https://doi.org/10.1109/JSTARS.2013.2257697